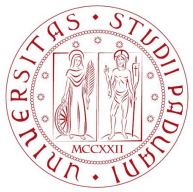

Università degli Studi di Padova

Dipartimento di Ingegneria dell'Informazione

Corso di Laurea in Ingegneria delle Telecomunicazioni

Thesis on

Interference Alignment Techniques for Multi-User MIMO Systems at Millimeter-Wave

Author

Stefano Ciccotosto

Supervisor

Prof. Nevio Benvenuto

Co-supervisor

Dr. Paolo Baracca

Padova, March 10, 2015

Academic Year 2014/2015

Una dedica speciale alla mia famiglia e ad Anna Isabella
per il costante sostegno durante gli anni universitari.

Abstract

The high number of nowadays applications using the wireless channel to exchange information among separate entities and the increasing bandwidth required by a single device make reasonable to start looking at the 30-300 GHz spectrum (corresponding to wavelength of the order of millimeters) for mobile broadband applications. In fact, almost all modern wireless communication systems use spectrum in the range of 300 MHz - 30 GHz, for reasons like fading-related issues as well as efficiency and cost of electronic components. However, research on multiple antennas communication gives interesting solutions to deal with such issues and offer the same advantages in terms of data rates and user multiplexing. In this work a review of the state-of-the-art of modern multi-user MIMO systems is given, presenting various algorithms that use interference alignment techniques to allocate multiple users over the same physical channel. In particular, the performance achieved with these methods over the millimeter-wave and the Rayleigh fading channels are compared and some considerations are given. Finally, the work is completed with the description of a novel frequency domain non-linear equalizer for wideband channels that combines the advantages of fractionally spaced equalization, non-linear processing and frequency domain implementation.

Contents

Notation

Symbol	Description
$\mathbf{x}$	Column vector
$\mathbf{X}$	Matrix
$\mathbf{X}^T$	Transpose of $\mathbf{X}$
$\mathbf{X}^*$	Complex Conjugate of $\mathbf{X}$
$\mathbf{X}^H$	Transpose Complex Conjugate (or Hermitian) of $\mathbf{X}$
$\mathbf{I}_n$	Identity matrix of dimension $n \times n$
$det(\mathbf{X})$	Determinant of matrix $\mathbf{X}$
$diag\{a_1, a_2, \cdots, a_n\}$	Diagonal matrix with diagonal elements $a_1, a_2, \cdots, a_n$
$\lvert \cdot \rvert$	Absolute value
$\lVert \cdot \rVert_2$	Frobenius norm
$\lambda^i_{min}(\mathbf{X})$	i-th smallest eigenvalue of matrix $\mathbf{X}$
$\nu^n_{min}(\mathbf{X})$	Matrix whose columns are the eigenvectors relative to the n smallest eigenvalues of $\mathbf{X}$
$E[\cdot]$	Expectation
$tr(\cdot)$	Trace operator
$gs(\cdot)$	Gram-Schmidt orthogonalization
$\Re(\cdot)$	Real part operator
$\Im(\cdot)$	Imaginary part operator

Acronyms

AoA	angle of arrival
AWGN	additive white gaussian noise
BD	block diagonalization
BER	bit error rate
BS	base station
CDF	cumulative distribution function
DFT	discrete Fourier transform
DL	downlink
DoF	degrees of freedom
FB	feedback
FD	frequency domain
FF	feedforward
FS	fractionally spaced
FS-IBDFE	FS iterative block decision feedback equalizer
HARQ	hybrid automatic repeat request
IA	interference alignment
IBDFE	iterative block DFE
i.i.d.	independent and identically distributed
IC	interference channel
IDFT	inverse discrete Fourier transform
INL	interference-plus-noise leakage
ISI	intersymbol interference
LDPC	low density parity check
LE	linear equalizer
MET	multiuser eigenmode transmission
MIMO	multiple input multiple output
MMSE	minimum mean-square error

MMW	millimeter-waves
MSE	mean-square error
NLOS	non-line-of-sight
NP-FS-FDE	noise prediction FS FD equalizer
OFDM	orthogonal frequency-division multiplexing
PP	point-to-point
PAPC	per-antenna power constraint
PCA	principal component analysis
PL	path loss
PN	pseudo noise
PSD	power spectral density
QPSK	quadrature phase shift keying
SNR	signal-to-noise ratio
SINR	signal-to-interference-plus-noise ratio
SPC	sum-power constraint
SVD	singular-value decomposition
TD	time domain
UHF	ultra high frequency
ULA	uniform linear array
UPA	uniform planar array
WSR	weighted sum-rate
ZF	zero forcing

Chapter 1

Introduction

Mobile communications play a key role in almost all recent technology innovations. With the increasing use of smart-phones and other portable data devices such as netbooks and tablets (Fig. 1.1), mobile data traffic is growing exponentially and new communication systems are needed to fullfill the bandwidth demand. The use of advanced technologies in the last years, like orthogonal frequency-division multiplexing (OFDM), multiple input multiple output (MIMO), turbo codes, hybrid automatic repeat request (HARQ) and many others have made possible to achieve higher spectral efficency and have brought data rates close to theoretical limits. On the other hand, as the spectral efficiency was reaching his limit, the accurate deployment of the network infrastructure exploited the possibility of frequency reuse over closer and closer locations by means of smaller cells and relays. However, because capacity can only scale linearly with the number of cells, small cells alone will not be able to meet the capacity required to accommodate orders of magnitude increases in mobile data traffic.

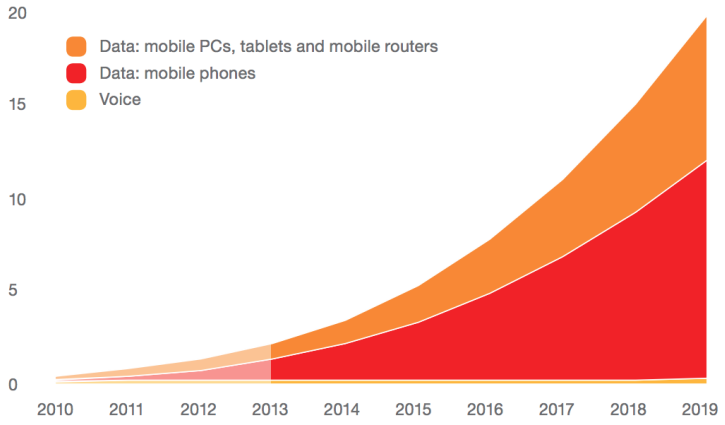

Figure 1.1: Global Mobile traffic (Montly ExaBytes) [1]

The allocation of unutilized spectrum can therefore represent a good solution, considering that nowadays almost all mobile communication systems use the portion of spectrum ranging from 300MHz to 30GHz and a vast amount of spectrum in the 30-300 GHz range remains unused. This band, know in the literature as millimeter-waves (MMW) band, is currently widely used for satellite communications and cellular backhauls. More recently, MMW transmissions have been used for very high throughput wireless LANs and personal area networks systems in the newly unlicensed 60 GHz bands. An overview of current allocated spectrum is available in Fig. 1.2. While

these systems offer rates in excess of 1 Gbps, the links are typically for short-range or point-to-point line-of-sight (LOS) settings [2].

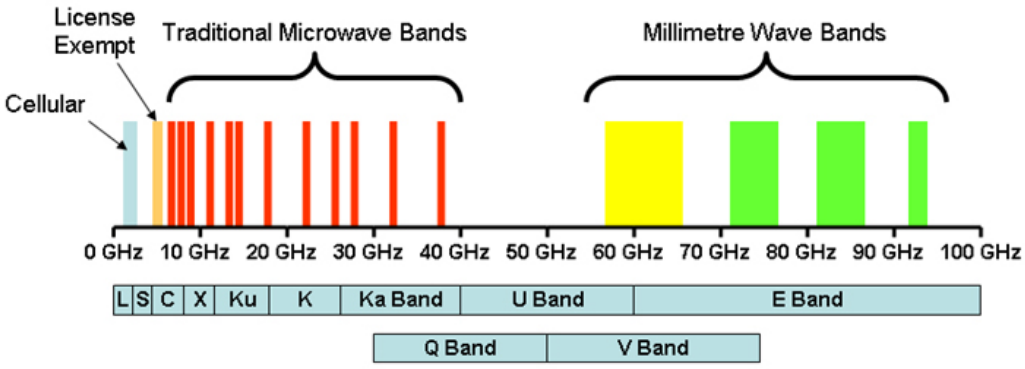

Figure 1.2: Current spectrum allocation.

In fact, there are still some doubt that MMW bands can be a viable solution for cellular systems that require reliable communications across long range and NLOS paths. The major concern is the increased transmission loss, due mainly by free space loss but also by the higher absorption rate of common material, compared to lower frequencies [3]-[4]. In fact, MMW signals do not penetrate most solid materials very well and transmissions can experience significant attenuations in the presence of heavy rain, because raindrops are roughly the same size as the radio wavelengths (millimeters) and therefore cause scattering of the radio signal [2]. Moreover, the presence of absorption bands of oxygen and water vapour limit the available bandwidth for commercial use. For example, the frequencies in the 57-64 GHz oxygen absorption band can experience attenuation of about $15dB/km$ as the oxygen molecule (O_2) absorbs electromegnetic energy at around $60GHz$ [5]. But even excluding these bands for broadband applications we can still have about 100GHz of available spectrum [6], and recent trends have encouraged a reconsideration of the viability of MMW cellular systems development despite the above mentioned issues.
In particular, as pointed out in [6], the concept of path loss lead to a general misunderstanding of the propagation phenomenon, making high frequencies considered disadvantaged compared to lower ones. This because the underlying assumption often used in radio engineering textbooks is that the path loss is calculated at a specific frequency between two isotropic antennas or $\lambda/2$ dipoles, whose effective aperture area increases with the wavelength (decreases with carrier frequency). As a result, a wider aperture area means that more energy is collected from a given radio signal. However, as the wavelength decrease, more antennas can be packed in the same area, resulting in no inherent disadvantage compared to longer wavelength in terms of free space loss. Multiple antenna transmission systems enable then to cope with the free space loss and, in addtion, result in higer gain trasmitters ad receivers thanks to the narrower beamform that they can generate.
Considering a typical urban environment, in fact, we have a twofold consequence: on one hand millimeter-wave signals do not penetrate most solid materials very well, determining a separation between indoor and outdoor communication and hindering non-line-of-sight (NLOS) links, but on the other hand reflection and diffraction behav-

iors actually facilitate NLOS communications because they reduce the number and the delay of incoming rays at the receiver. Furthermore, the Doppler shift caused by the dynamic of the working environment will have a lighter impact on signals while the narrow beams generated by the antenna array will significantly reduce angular spread of the incoming waves, which in turn reduces the Doppler spread [6].
We see then that the MMW spectrum owns a high potential for next generation mobile communication systems and that MIMO represent the leading technology that can possibly open to new interesting scenarios. This, togheter with coordination between cellular base station (BS) [7], will allow an efficiently exploitation of the channel resources and satisfy the bandwidth demand. In this work we will analyze the state-of-the-art of modern beamforming techniques for MIMO systems, focusing on those that enable the simultaneous transmission from a BS to many users (downlink (DL) scenario) and between several nodes couple (point-to-point (PP)). In particular, we aim at evaluating the performance given by different algorithms that try to suppress interference caused by simultaneous transmissions occurring between several users that share the same physical channel. Particular attention will be given to the behavior of such algorithms when employed over the MMW spectrum in order to appreciate differencies and issues of this particular band compared to the classical Rayleigh fading channel model (RYL) used in modern cellular systems. Moreover, in Chapter 7 it is presented a novel decision feedback equalizer in the frequency domain (FD) that achieves intersymbol interference (ISI) suppression present in broadband wireless transmissions. The proposed equalizer combines the advantages of fractionally spaced (FS) equalization, non-linear processing and FD implementation, giving furthermore a closed form expression of the equalizer coefficients. This last work has been submitted to the IEEE Wireless Communications Letter.

It is possible to find an introduction to MIMO communications in [8].

Chapter 2

Millimeter Wave Channel

The millimeter-wave spectrum, ranging between 30 and 300 GHz, shows substantial differencies in the propagation property compared with lower frequencies since elements like buildings, umidity and even foliage can represent serious attenuation factors that affect transmissions more heavily than in lower bands, as explained in [6]. On the other hand, the small size and separation (around half of the wavelength) of millimeter-wave antennas allow a large number of antennas to be packed in a relative small area (e.g., tens of antennas per square centimeter area at 80 GHz carrier frequency) and consequently a high beamforming gain can be reached. Additionally, a large number of antennas means that signal travels from Tx to Rx arrays across multiple high-gain narrow beams, so that we can model such channel as a combination of multiple rays received with the same delay but different phases. In the following chapter, we will cover some of the propagation aspects of MMW and the mathematical model that can efficiently describe them in order to understand resources and issues of this particular band.

2.1 Characterization of propagation

In a classical propagation scenario, power attenuation is usually modeled by means of the path loss (PL) formula, where the average received power is estimated by combining the expression of free-space attenuation with the gain of the antennas involved in the communication. If an obstruction is present, then the received signal will suffer additional attenuation. Equation (2.1) accounts for attenuation factors caused by obstructive elements such as rain, foliage and windows glass that are particularly relevant in the MMW channel [9]. Moreover, since directional antennas are considered, the relative gains will depend on the azimuth (ϕ) and elevation (θ) angles of the transmitted and received rays [10]. The final PL equation for the MMW channel assumes then the form

$$\begin{aligned} P_r[dBm] = P_t[dBm] - 10\alpha log\left(\frac{4\pi d}{\lambda}\right) + \Lambda_t(\phi_t,\theta_t)[dB] + \Lambda_r(\phi_t,\theta_t)[dB] + \\ - A_o[dB] - A_w[dB] - A_m[dB] \end{aligned} \tag{2.1}$$

with

- $\lambda = c/f_c$ Wavelengh at carrier frequency f_c;

- d Path length;
- α Decay slope;
- Λ_t Transmitter directional gain as a function of the azimuth ϕ_t and elevation θ_t angles;
- Λ_r Receiver directional gain as a function of the azimuth ϕ_t and elevation θ_t angles;
- A_o Average attenuation caused by oxygen absorption;
- A_w Average attenuation caused by weather conditions (rain, moisture, hail...);
- A_m Average attenuation caused by general material such as foliage and window glass.

In typical models used at UHF the decay of power due to separation between users is generally dependent on the environment characteristics and on reference distances. This results in very simple models, usually based on the interference of a direct and a ground-reflected ray, as shown in Fig. 2.1, with a simple dependence of the power on the distance d of the type $10\alpha log(d)$, as in (2.1). While in UHF this model usually lead to $\alpha = 4$ instead of $\alpha = 2$ as in the free-space propagation, at higher frequency this is not necessarily satisfied. In fact, as explained in [5], one of the conditions to be satisfied is that the path length difference between the direct and reflected rays is less than $\lambda/2$, which defines the break-point distance, $d_{bp} = 4h_t h_r/\lambda$ (h_t and h_r are the transmit and receive antenna heights, respectively), beyond which the fourth power law has to be used. In millimeter wave case, assuming frequency ranging from 60 to 66 GHz, $h_r = 1.8m$ and $h_t \in [5, 50]\, m$, we get $d_{bp} \in [7.2, 72.9]\, Km$, which is far beyond the expected maximum range for the cell radius (from 0.5 up to 1 Km). We can therefore assume $\alpha = 2$ for the mm-wave signals, as confirmed by measurements performed in [5].

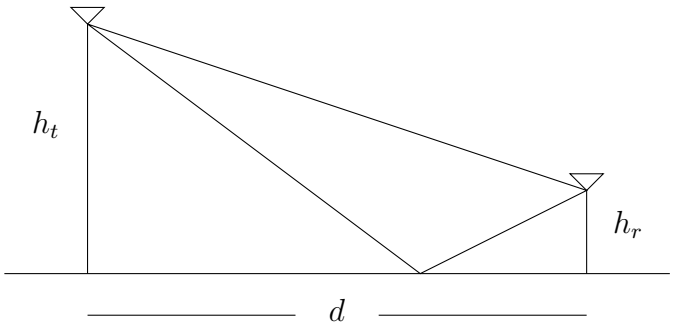

Figure 2.1: Two-rays propagation model.

The path loss exponent α is useful for predicting large scale propagation effects. However, it is inadequate at predicting site-specific propagation effects, such as reflection, diffraction, or penetration losses caused by a particular building layout, construction materials, furniture, etc.
As reported in (2.1), high attention should be paid to attenuation factors that significantly affect the propagation besides the normal fading due to distance. In fact, the

chemical composition of the atmosphere can present reasonance effects that dissipate signal energy. For example, around 60 GHz we found a peak of attenuation caused by oxygen reasonance phenomena that in general is not negligible over the bandwidth of our interest. In [5], the following sperimental model for the oxygen is developed

$$A_{o[dB/Km]}\left(f_{c[GHz]}\right) = \begin{cases} 0.104(f_c - 60)^{3.26} - 15.10 & 60 \leq f_c \leq 63 \\ 11.35 + (f_c - 63)^{2.25} - 5.33(f_c - 63)^{1.27} & 63 < f_c \leq 66 \end{cases}$$

Moreover, weather condition may also affect significantly propagation, but while the influence of water vapour absorption, fog, hail, snow, sand, etc. can be neglected, either because the attenuation coefficient is very low or because these events occur with very low probability, attenuation due to rain can also be of some importance in the MMW band, depending on the rainfall rate $R_{[mm/h]}$. Again in [5], the following model is given for the rain attenuation

$$A_{r\,[dB/Km]}\left(f_{c[GHz]}, R_{[mm/h]}\right) = k(f)R^{a(f)} \tag{2.2}$$

where $k(f)$ and $a(f)$ are approximately equal to

$$k(f) = 10^{1.203\log(f)-2.29}, \qquad a(f) = 1.703 - 0.493\log(f). \tag{2.3}$$

It is remarked in [5] that rain can play an important role in cell coverage reduction, since its attenuation can reach values larger than those for oxygen, depending on the rainfall rate (18 dB/km for 50 mm/h), while oxygen and rain attenuations cannot be neglected if large distances (>1 km) are to be considered, but for calculations within cells (with ranges less than 200 m) they may not be of great importance.
In Figure 2.2 it is plotted the attenuation values due to atmospheric condition as a function of the frequency and it is easy to note the peaks caused by the absorption bands of oxygen and moisture.

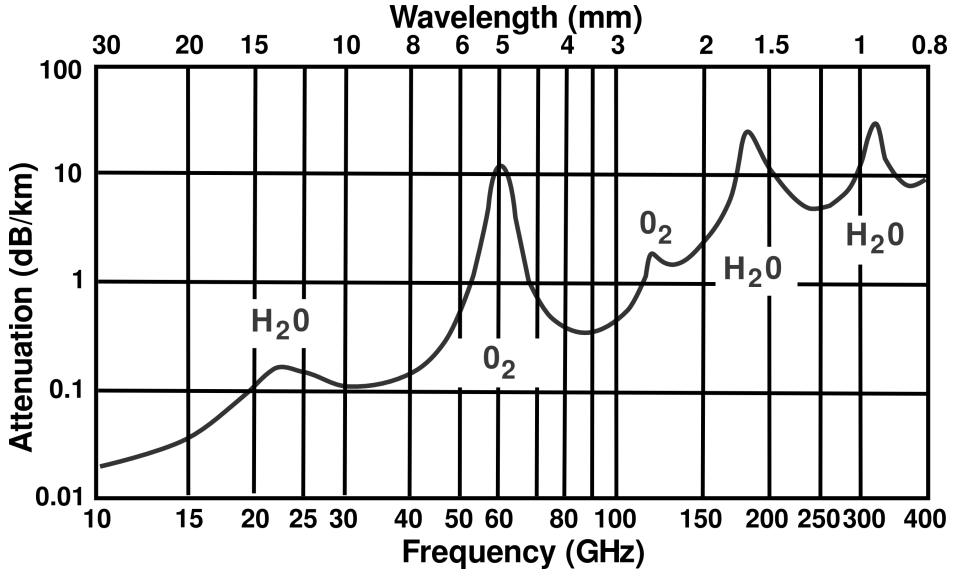

Figure 2.2: Atmospheric attenuation as a function of the carrier frequency.

We end our dissertation about outdoor attenuation agents with the effect of foliage on propagation. In fact, foliage losses for millimeter waves are significant and can be a limiting impairment for propagation in some cases. An empirical formula has been reported in [11] to calculate the propagation through foliage

$$A_f = \frac{(f)^{0.3} D^{0.6}}{5}, \tag{2.4}$$

where D is the depth of foliage area between transmitter and receiver.

		Drywall	Office Whiteboard	Clear Glass	Mesh Glass	Clutter
Material Thickness (cm)		2.5	1.9	0.3	0.3	–
2.5 Ghz	Average Measured Attenuation (dB)	5.4	0.5	6.4	7.7	2.5
	Measurement Standard Deviation (dB)	2.1	2.3	1.9	1.4	2.2
	Normalized Average Attenuation (dB/cm)	2.1	0.3	20.0	24.1	–
60 Ghz	Average Measured Attenuation (dB)	6.0	9.6	3.6	10.2	1.2
	Measurement Standard Deviation (dB)	3.4	1.3	2.2	2.1	1.8
	Normalized Average Attenuation (dB/cm)	2.4	5.0	11.3	31.9	–

Table 2.1: Loos in excess of free-space at 2.5 and 60 GHz for indoor signal propagation [3].

Indoor coverage deserves a separate discussion as signal penetration of building can be really weak because of the large attenuation factor of walls and windows. The use of indoor femtocells could then be needed to extend cellular signal, and the coverage limit just mentioned could possibly lead to higher frequency reuse rate between adjacent rooms or buildings. In Table 2.1, the attenuation values for 2.5 and 60 GHz are reported for common indoor material such as walls, clear glass, mesh glass (reinforced windows), whiteboard and objects that do not directly block the LOS signal from transmitter to receiver but somehow interfere with the propagation, defined as clutter. Clutter includes office furniture such as chairs, desks, bookcases, and filing cabinets. Comparing the measured losses, taken from [3], for 2.5 and 60 GHz in Table 2.1, the attenuation of drywall, whiteboard, and mesh glass increases from 2.5 to 60 GHz; however, the attenuation of clear glass and clutter decreases. The reason for the decrease in attenuation from clutter is explainable by the fact that with narrower beams, fewer objects in the environment are capable of perturbing the LOS signal. It is not known why the attenuation of Clear Glass, decreases from 2.5 to 60 GHz. It has been also noticed that when using highly directional antennas at 60 GHz, the large-scale mean path loss is very close to free space, confirming the results presented in [5], but the spread of values about the mean is higher than at 2.5 GHz. Moreover, the RMS delay spread at 2.5 GHz is significantly higher than at 60 GHz, due to the use

of omnidirectional antennas at 2.5 GHz and directional antennas at 60 GHz [3]. This can be caused by the high attenuation of reflecting materials, that limits the number of path through which the signal can travel without excessive attenuation, enabling therefore higher data rates communications.
Further attenuation values are provided in [4], and here reported in Table 2.2, where is also highlighted the dependence on the polarization of the incident wave, as a consequence of an internal oriented structure of materials.

Material	$d_s(mm)$	$A_h[dB]$	$A_v[dB]$	**Material**	$d_s(mm)$	$A_h[dB]$	$A_v[dB]$
Chipwood	16	7.9	8.6	Mortar	100	159.98	159.3
Glass	4	3.1	2.5	Brick Wall	100	177.92	195.06
Wood	7	2.6	3.5	Concrete	100	174.95	178.05
Plasterboard	15	2.7	2.9				

Table 2.2: Attenuation values for different materials and with horizontal (A_h) and vertical (A_v) polarization at 40GHz [4].

2.2 MIMO Channel Models

In the following section we present the model that will be used in this thesis as from [10]. The equivalent complex base band impulse response of a MMW MIMO channel with narrow impulses can be represented by a matrix $\mathbb{C}^{N\times M}$ of the form

$$\mathbf{H} = \begin{bmatrix} h_{1,1} & \cdots & h_{1,M} \\ \vdots & \ddots & \vdots \\ h_{N,1} & \cdots & h_{N,M} \end{bmatrix} \tag{2.5}$$

where $h_{i,j}$ are complex random variables satisfying

$$\mathbb{E}\left[\|\mathbf{H}\|^2\right] = MN. \tag{2.6}$$

In the following paragraphs we will show how to get (2.5) from the configuration of the antenna arrays considered.

2.2.1 Uniform Linear Array

Consider a MIMO channel with two linear arrays composed by M and N antennas, respectively, at Tx and Rx side. For both arrays, the inter-antenna spacing is equal to half the signal wavelength λ, and the array axe lies in the azimuth plane that will therefore contain the rays generated by the array. We refer to this configuration as uniform linear array (ULA).
For an ULA and for a given ray, let consider a column vector of phasors

$$\mathbf{a}(\phi) = \frac{1}{\sqrt{N}}\left[1 \;\; e^{j\psi D\sin\phi} \;\; \cdots \;\; e^{j(N-1)\psi D\sin\phi}\right]^T \tag{2.7}$$

being $\psi = 2\pi/\lambda$, $D = \lambda/2$ the inter-antenna spacing and ϕ the angle of departure or arrival of the ray, depending if we consider Tx or Rx side. If L rays are received with the same delay, the channel matrix introduced in (2.5) can be rearranged considering vector (2.7) in the following way

$$\mathbf{H}_{ULA} = \sqrt{\frac{MN}{L}} \sum_{l=1}^{L} g_l \mathbf{a}_r \left(\phi_l^{(r)}\right) \mathbf{a}_t^H \left(\phi_l^{(t)}\right) \tag{2.8}$$

where $\mathbf{a}_r$ and $\mathbf{a}_t$ are as in (2.7) for Rx and Tx, respectively, and $g_l \sim \mathcal{CN}(0,1)$ represent the complex random gain of the ray l. We highlight that from the definition of $\mathbf{a}$ as in (2.7), elements of (2.8) are determined by the phase offset of the different rays due to the relative position across array elements, as depicted in Figure 2.3.
For simplicity, we rewrite (2.8) into a matrix formulation with the aid of the following matrices

$$\mathbf{A}_t = \left[\mathbf{a}_t\left(\phi_1^{(t)}\right) \quad \mathbf{a}_t\left(\phi_2^{(t)}\right) \quad \cdots \quad \mathbf{a}_t\left(\phi_L^{(t)}\right)\right]^T \tag{2.9}$$

$$\mathbf{A}_r = \left[\mathbf{a}_r\left(\phi_1^{(r)}\right) \quad \mathbf{a}_r\left(\phi_2^{(r)}\right) \quad \cdots \quad \mathbf{a}_r\left(\phi_L^{(r)}\right)\right]^T \tag{2.10}$$

$$\mathbf{H}_g = diag\left(g_1, g_2, \cdots, g_L\right) \tag{2.11}$$

and

$$\mathbf{H} = \sqrt{\frac{MN}{L}} \mathbf{A}_r \mathbf{H}_g \mathbf{A}_t^H \tag{2.12}$$

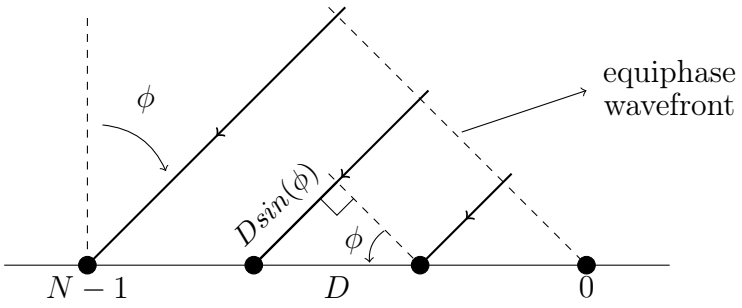

Figure 2.3: Relative path difference in an ULA.

2.2.2 Correlation of the ULA channel

The peculiarity of the channel considered in this work is the high correlation between adjacent elements of the antenna array. The expression for the correlation at Tx and Rx are given by the followings

$$\mathbf{R}_{TX} = E\left[\mathbf{H}^H\mathbf{H}\right] \quad \textit{and} \quad \mathbf{R}_{RX} = E\left[\mathbf{H}\mathbf{H}^H\right]. \tag{2.13}$$

By expanding the expectation it is possible to get a closed-form for a generic entry on row p and column q of the Tx correlation matrix

$$[\mathbf{R}_{TX}]_{p,q} = \frac{N}{\phi_{max} - \phi_{min}} \int_{\phi_{min}}^{\phi_{max}} e^{j\psi(p-q)sin(a)} da \tag{2.14}$$

and the Rx correlation matrix

$$[\mathbf{R}_{RX}]_{p,q} = \frac{M}{\phi_{max} - \phi_{min}} \int_{\phi_{min}}^{\phi_{max}} e^{j\psi(p-q)sin(a)} da. \tag{2.15}$$

2.2.3 Uniform Planar Array

Similar results can be found when considering arrays spanning two dimensions, composed by $N = WH$ antennas, with inter-element space equal to D, where W and H are the antennas composing the single dimension. Also in this case we define the phase vector as

$$\mathbf{b}(\phi, \theta) = \frac{1}{\sqrt{L}} \left[1 \cdots e^{j\psi D(w \sin\phi \sin\theta + h\cos\theta)} \cdots e^{j\psi D((W-1)\sin\phi\sin\theta + (H-1)\cos\theta)}\right]^T \tag{2.16}$$

where $w = 1, .., W-1$ and $h = 1, ..., H-1$ are the antenna index, $\psi = 2\pi/\lambda$ and $D = \lambda/2$. With the vector just defined we can generate the $N \times M$ channel impulse response, valid for a uniform planar array (UPA) system, as in (2.8), obtaining the matrix

$$\mathbf{H}_{UPA} = \sqrt{\frac{MN}{L}} \sum_{l=1}^{L} g_l \mathbf{b}_r \left(\phi_l^{(r)}, \theta_l^{(r)}\right) \mathbf{b}_t^H \left(\phi_l^{(t)}, \theta_l^{(t)}\right) \tag{2.17}$$

We can note that, with UPA, beamforming in elevation is also possible since the channel impulse response is function of the parameter θ.
A matrix formulation is again useful, so by defining

$$\mathbf{B}_t = \left[\mathbf{b}_t\left(\phi_1^{(t)}, \theta_1^{(t)}\right) \quad \mathbf{b}_t\left(\phi_2^{(t)}, \Theta_2^{(t)}\right) \quad \cdots \quad \mathbf{b}_t\left(\phi_L^{(t)}, \theta_L^{(t)}\right)\right]^T \tag{2.18}$$

$$\mathbf{B}_r = \left[\mathbf{b}_r\left(\phi_1^{(r)}, \theta_1^{(r)}\right) \quad \mathbf{b}_r\left(\phi_2^{(r)}, \theta_2^{(r)}\right) \quad \cdots \quad \mathbf{b}_r\left(\phi_L^{(r)}, \theta_L^{(r)}\right)\right]^T \tag{2.19}$$

$$\mathbf{H}_g = diag\left(g_1, g_2, \cdots, g_L\right) \tag{2.20}$$

we rewrite (2.17) as

$$\mathbf{H} = \sqrt{\frac{MN}{L}} \mathbf{B}_r \mathbf{H}_g \mathbf{B}_t^H \tag{2.21}$$

Chapter 3

Scenario

3.1 System description

As illustrated in Fig. 3.1, our system is a K-user MIMO interference channel (IC), where K transmitters (Tx's), each equipped with M antennas, transmit to K receiver (Rx's), each equipped with N antennas, simultaneously, so that transmissions are supposed to happen between the pair of Tx/Rx with the same index, i.e. from transmitter k to receiver k. Furthermore, for a given user, d parallel streams are allocated. The channel is supposed narrow-band so that each transmitter-receiver link will experience quasi-static fading, time-invariant over each transmission duration and different among successive transmissions.

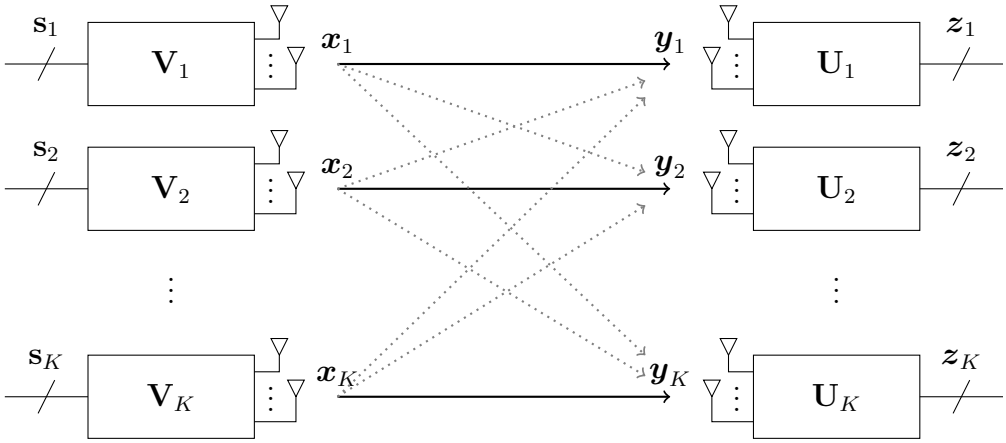

Figure 3.1: System configuration.

For each symbol s_k^l, belonging to stream l of user k, linear precoding is performed independently at each channel realization. By definining the precoding column vector for stream l as $\mathbf{v}_k^l$, the transmitted signal of user k obtained by summing all the streams assumes the form (see also Fig. 3.2):

$$\mathbf{x}_k = \sum_{l=1}^{d} \mathbf{x}_k^l = \sum_{l=1}^{d} \mathbf{v}_k^l s_k^l. \tag{3.1}$$

A unitary sum-power constraint (SPC) for each user is considered, so that the total available power P_k is distribute among the streams belogning to user k for which the transmitted power assumes the form

$$E\left[\|\mathbf{x}_k^l\|_F^2\right] = \rho_k^l P_k \tag{3.2}$$

with $\sum_{l=0}^{d} \rho_k^l = 1$ for any $k \in \{1, \cdots, K\}$. If *power allocation* is not employed, each stream will share a equal fraction of the total power, i.e. $\rho_k^l = 1/d$, while if interference suppression is achieved, a more efficinet use of the channel would require a water-filling algorithm (Appendix A) to allocate power across the streams of a given user.
Assuming data symbols to have unitary power, (3.2) implies $\|\mathbf{v}_k^l\|_2^2 = \rho_k^l P_k$. For simplicity we will assume $P_k = 1, \forall k \in \{1, \cdots, K\}$.
By further defining $\mathbf{H}_{k,j}$ as the $N \times M$ MIMO channel matrix from transmitter j to receiver k and $\mathbf{n}_k \sim \mathcal{CN}(0, \sigma_w^2)$ as the complex zero-mean Gaussian noise affecting user k, with covariance matrix

$$\mathbf{\Xi}_k = E\left[\mathbf{n}_k^H \mathbf{n}_k\right] = \sigma_w^2 \mathbf{I}_N, \tag{3.3}$$

the signal vector received by receiver k, is equal to:

$$\mathbf{y}_k = \sum_{j=1}^{K} \sum_{n=1}^{d} \mathbf{H}_{k,j} \mathbf{x}_j^n + \mathbf{n}_k \tag{3.4}$$

with $k \in \{1, \cdots, K\}$.

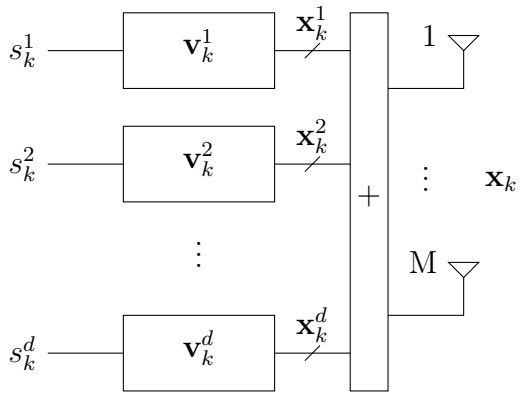

Figure 3.2: Particular of transmitter k structure (beamformer).

It is furthermore assumed that:

1. all transmitters generate independent identically distributed (i.i.d.) data symbols, *i.e.* $E\left[(s_j^n)^* s_k^l\right] = 0$ for $(j,n) \neq (k,l)$;

2. all transmitted signals are statistically-independent of the noise at the receiver, *i.e.* $E\left[(\mathbf{x}_j^n)^H \mathbf{n}_k\right] = 0$ for all $k, j \in \{1, \cdots, K\}$ and $n \in \{1, \cdots, d\}$.

At the receiver side, as shown in Fig. 3.3, stream l associated to user k is filtered by a linear structure (combiner), a $1 \times N$ vector denoted as $(\mathbf{u}_k^l)^H$, which finally leads to the signal at detection point, given by:

$$z_k^l = \left(\mathbf{u}_k^l\right)^H \mathbf{y}_k = (\mathbf{u}_k^l)^H \mathbf{H}_{k,j} \mathbf{x}_j^n + \sum_{(j,n)\neq(k,l)} (\mathbf{u}_k^l)^H \mathbf{H}_{k,j} \mathbf{x}_j^n + (\mathbf{u}_k^l)^H \mathbf{n}_k. \tag{3.5}$$

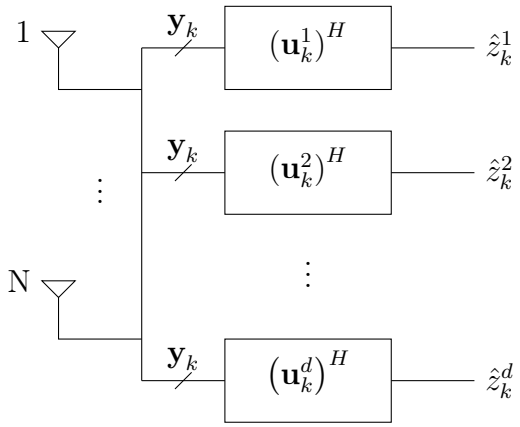

Figure 3.3: Particular of the receiver k structure (combiner).

In (3.5) it is highlighted the contribution of the useful signal against the contribution of intra-user and inter-user interference plus noise.
From (3.5), we derive the statistical power of the total *interference leakage* plus noise at detection point for stream l of user k, equal to

$$I_k^l = \left(\mathbf{u}_k^l\right)^H \mathbf{\Xi}_k \mathbf{u}_k^l + \sum_{(j,n)\neq(k,l)} \left| \left(\mathbf{u}_k^l\right)^H \mathbf{H}_{k,j} \mathbf{v}_j^n \right|^2, \tag{3.6}$$

for which the relative signal-to-interference-plus-noise ratio (SINR) is defined as

$$\Gamma_k^l = \frac{|\left(\mathbf{u}_k^l\right)^H \mathbf{H}_{k,k} \mathbf{v}_k^l|^2}{I_k^l}. \tag{3.7}$$

The associated achievable rate will then have the form

$$\mathcal{R}_k^l = \log_2\left(1 + \Gamma_k^l\right). \tag{3.8}$$

For simplicity, we will eventually consider the symbol vector of user k as the column vector whose elements are the symbols belonging to the d streams and consequently use a matrix notation to denote beamformers and combiners in some of the presented algorithms, i.e. we set

$$\mathbf{s}_k = \left[s_k^1, \cdots, s_k^d\right]^T, \tag{3.9}$$

$$\mathbf{z}_k = \left[z_k^1, \cdots, z_k^d\right]^T, \tag{3.10}$$

$$\mathbf{V}_k = \left[\mathbf{v}_k^1, \cdots, \mathbf{v}_k^d\right], \tag{3.11}$$

$$\mathbf{U}_k = \left[\mathbf{u}_k^1, \cdots, \mathbf{u}_k^d\right]. \tag{3.12}$$

In this case, (3.4) and (3.5) become, respectively,

$$\mathbf{y}_k = \sum_{j=1}^{K} \mathbf{H}_{k,j} \mathbf{V}_j \mathbf{s}_k + \mathbf{n}_k \tag{3.13}$$

$$\mathbf{z}_k = \mathbf{U}_k^H \mathbf{y}_k. \tag{3.14}$$

and, consequently, (3.6), (3.7) and (3.8) assume a per-user form, i.e.

$$\mathbf{I}_k = \mathbf{U}_k^H \mathbf{\Xi}_k \mathbf{U}_k + \sum_{j \neq k} \left[\mathbf{U}_k^H \mathbf{H}_{k,j} \mathbf{V}_j \mathbf{V}_j^H \mathbf{H}_{k,j}^H \mathbf{U}_k \right], \tag{3.15}$$

$$\mathbf{\Gamma}_k = \mathbf{I}_k^{-1} \left[\mathbf{U}_k^H \mathbf{H}_{k,k} \mathbf{V}_k \mathbf{V}_k^H \mathbf{H}_{k,k}^H \mathbf{U}_k \right] \tag{3.16}$$

$$\mathcal{R}_k = \log_2 \left[det \left(\mathbf{I} + \mathbf{\Gamma}_k \right) \right]. \tag{3.17}$$

Finally, if instead of having K separate transmitters we have just a single transmitter, e.g. a base station, all the formulas still hold by assuming

$$\mathbf{H}_{k,1} = \mathbf{H}_{k,2} = \cdots = \mathbf{H}_{k,K} = \mathbf{H}_k, \quad k \in \{1, \cdots, K\} \tag{3.18}$$

so that the single subscript will mean that a single transmitter scheme is being assumed.

3.2 Interference Alignment

In the K users interference channel, the key idea for interference suppression, when its power is comparable to the desired signal, is channel orthogonalization. This is also the basis for codes, time or frequency division channel access schemes that avoid interference between coexisting users by dividing time or spectrum in a cake-cutting fashion. In general, interference alignment (IA) scheme is extending the idea of orthogonality to the space dimensions, through beamforming across multiple antennas.
The enabling premise for interference alignment in all the preceding examples is the relativity of alignment, i.e. the alignment of signal vector spaces is relative to the observer. Two transmitters may appear to be accessing the channel simultaneously to one receiver while they appear to be orthogonal to another receiver. Since each receiver has a different view, there exist scenarios where each receiver, from its own perspective, appears to be privileged relative to others. The goal of IA is to create such scenarios in a wireless network. Specifically, IA refers to a construction of signals in such a manner that they cast overlapping shadows at the receivers where they constitute interference while they remain distinguishable at the receivers where they are desired [12].

More in depth, from (3.14) the condition targeted by IA is the following

$$\mathbf{U}_k^H \mathbf{H}_{k,j} \mathbf{V}_j = \mathbf{0} \quad for\ j \neq k. \tag{3.19}$$

In this situation, a receiver can easily cancel several interferers since they are all aligned to a specific subspace of the received signal space, and (3.14) simplify in

$$\mathbf{z}_k = \mathbf{U}_k^H \mathbf{y}_k = \mathbf{U}_k^H \mathbf{H}_{k,j} \mathbf{x}_j + \mathbf{U}_k^H \mathbf{n}_k. \tag{3.20}$$

In order to achieve condition (3.19), cooperation among users is necessary, meaning that each Tx should care about the interference caused to other Rx's and not just aim at maximizing its own transmissions (3.7).
IA is a cooperative strategy that can achieve the channel capacity, but its drawback is that in general a closed form solution for beamformers and combiners design is available only in few simple cases and under the assumption of perfect channel knowledge. In

fact, iterative algorithms are often required to reach optimum, so that beamformers and equalizers are alternatively updated to reach condition (3.19). Moreover, perfect alignment is not alway possible and it is still not clear the feasibility of alignment for a signal space with a *limited* number of dimensions [13]. For that reason, IA under perfect alignment often results in suboptimal sum-rate at moderate signal-to-noise ratio (SNR), and relaxing the zero-forcing constraint is sometimes needed to converge to a solution that actually achieves better rates, especially with an increasing number of users.

In [12], it is shown that for a MIMO IC the theoretical achievable rate with IA is $\frac{KN_a}{2}\log(\Gamma) + o(log(\Gamma))$, with Γ as in (3.7) and with $N_a = M = N$. This means that the achievable rate of the single user in the IC could be half of what would have been in the absence of interference.

To give a pictorial representation on how IA works, in Fig. 3.4 is reported an example for a 3-dimensional signal space. As we previously stated, the IA conditions imply that we need to align the interference at each receiver by occupying an $(N-d)$-dimensional subspace, creating an interference-free, d-dimensional space for the desired signal. Equivalently, if we are able to create at each receiver a d-dimensional signal space that is free from interference, we have implicitly aligned the interference in the other remaining space. This done, all a receiver has to do is to hide from the interference by projecting the received signal onto the d-dimensional subspace that has the lowest interference, thereby suppressing all the undesired interference [14].

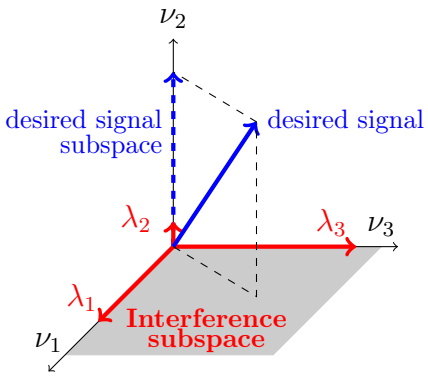

Figure 3.4: Example of a 3-D signal space.

We might wonder what is then a suitable mathematical tool that can allow us to measure the interference level along each signal dimension. We know from principal component analysis (PCA) that the eigenvectors of the interference covariance matrix correspond to the dimensions along which a receiver "sees" interference, and their corresponding eigenvalues indicate the variance / power of interference along that dimension (Fig. 3.4). Assuming that the eigenvalues and their corresponding eigenvectors are sorted in increasing order, this implies that the d dimensional subspace with the lowest interference is spanned by the d eigenvectors corresponding to the d smallest eigenvalues, and the variance of interference in this subspace is given by the sum of the d smallest eigenvalues [14].

In order to give the idea of how PCA can be applied to IA, a simple iterative algorithm, presented in [13], is described below. For a given set of beamformers $\mathbf{V}_k$, we can rewrite the expression of the *interference leakage* (the second term of (3.6)) as

$$\mathcal{I}_k = \|\mathbf{U}_k^* \mathbf{\Theta}_k \mathbf{U}_k\|_F^2 \tag{3.21}$$

being

$$\mathbf{\Theta}_k = \sum_{j \neq k} \mathbf{H}_{k,j} \mathbf{V}_j \mathbf{V}_j^* \mathbf{H}_{k,j}^* \tag{3.22}$$

the received interference covariance matrix. To minimize the contribution of (3.22) in (3.6), the combiner should be aligned to the subspace where (3.22) is minimum. The d dimensional received signal subspace that contains the least interference is the space spanned by the eigenvectors corresponding to the d smallest eigenvalues of the interference covariance matrix (3.22), that is

$$\mathbf{U}_k = \nu_{min}^d \left(\mathbf{\Theta}_k \right). \tag{3.23}$$

Once the combiner is set, we consider the reciprocal channel, i.e. the channel obtained by switching the role of Rx and Tx, and whose channel matrix is given by the Hermitian transposition of the direct channel, i.e.

$$\overleftarrow{\mathbf{H}}_{k,j} = \mathbf{H}_{j,k}^H, \quad j,k \in \{1, \cdots, K\}. \tag{3.24}$$

By considering (3.23) as beamformer, i.e.

$$\overleftarrow{\mathbf{V}}_k = \mathbf{U}_k \tag{3.25}$$

where the arrow is referring to the reciprocal channel, we can now apply relation (3.23) to update combiners for the reciprocal channel, that is

$$\overleftarrow{\mathbf{U}}_k = \nu_{min}^d \left(\overleftarrow{\mathbf{\Theta}}_k \right). \tag{3.26}$$

We can now turn back to the direct channel, upating the old beamformer used in the previous iteration with the combiner just found, obtaining

$$\mathbf{V}_k = \overleftarrow{\mathbf{U}}_k, \tag{3.27}$$

and alternate direct and reverse channel with the update rule (3.23) until convergence is reached.
The idea behind (3.25) is that if the signal subspace over which $\mathbf{U}_k$ is defined is lightly affected by interference, transmitting on the same signal subspace will cause the least interference to other users. The result is that each transmitter will adjust its beamformer to cause the least possible interference to non-intended users, while receivers will "hear" the channel over the subspace with less interference. The drawback of this method is that, in general, the interference free subspace found by one user may not be a lucky one for its own transmission because of the low gain provided by the selected modes. In that sense seeking only for interference avoidance can be not optimal for the whole systems, especially at low SNR. Allowing therefore a little amount of interference can sometimes give an overall gain in terms of SINR. Other strategies can therefore be employed, to maximize quantities such as the SINR or the total sum-rate of the system instead of simply avoiding interference, as we will show later.

3.3 Simulation Setup

In this work, we aim at evaluate the overall system sum-rate achieved after interference has been canceled or reduced, summing the singular rates reached by each user given by 3.28, that is equal to

$$\mathcal{R} = \sum_{k=1}^{K} \sum_{l=1}^{d} \log_2 \left(1 + \Gamma_k^l\right) \tag{3.28}$$

with Γ_k^l as in (3.7).
For each realization, channel matrix for the direct and cross links are generated independently. For the MMW case, the channel matrix is as in Section 2.2, while the classical Rayleigh channel matrix is composed by independent and identically distributed (i.i.d.) entries taken randomly from a complex Gaussian distribution with zero mean and unit power.
For our purposes, we do not consider distances nor eventual blocking object between each pair Tx/Rx.
The results obtained will then be presented by plotting the system sum-rate (expressed in $bit/s/Hz$) against the SNR, defined as $1/\sigma_w^2$, being unitary both the Tx power and also each channel gain. For each figure, the following parameters will be defined:

- K: the number of Rx users;
- K_{Tx}: number of Tx users ($K_{Tx} = K$ in point-to-point configuration, $K_{Tx} = 1$ in downlink configuration);
- N: number of Tx antennas;
- M: number of Rx antennas;
- SPC: waterfilling algorithm is used for power allocation.

Chapter 4

Combiner design methods

In this chapter, we cover combiner design, giving different approaches to the problem of aligning the receiver subspace to match as much as possible the transmitter one. Normally these filters have a simpler form than that of the beamformers, since they are usually implemented in portable devices for which energy consumption and processing complexity represent important factors that affect implementation decisions. For this reason, in the IA algorithms that we will present the receivers are in some case fixed and the design is concentrated on transmitters.

4.1 Principal/Singular Components Analysis

We start with the most simple design method for combiners, that is to use principal/singular decomposition of the channel matrix. An example of this approach has been already employed in Section 3.2 to avoid interference, but in general, if applied to the direct channel matrix, it could lead to a very simple alignment that is certainly favourable for the intended signal that is received over the highest gain direction. Although this is a very immediate solution and it does not require knowledge from other users but only on the direct channel matrix, its drawbacks are that in general computing eigen or singular vectors has a high computational complexity. Moreover the resulting combiner does not participate to the interference alignment process since no consideration is given to cross channel matrix. However, this choice represents the best possible solution for low SNR, as stated in [15], and it is also a good solution for the initialization of combiners in iterative algorithms.

4.2 Interference Rejection

In [16], signal received from each user antenna is weighted and combined in order to maximize the SINR at the detection point.
Indeed, the receiver front-end multiplies signal by a weight obtained from the noise-plus-interference correlation matrix

$$\mathbf{\Psi}_k = E\left[\left(\sum_{j\neq k}\mathbf{H}_k\mathbf{x}_j + \mathbf{n}_k\right)^*\left(\sum_{j\neq k}\mathbf{H}_k\mathbf{x}_j + \mathbf{n}_k\right)^T\right]. \tag{4.1}$$

that in case of uncorrelation between noise and interference simplifies in

$$\mathbf{\Psi}_k = \sigma_w^2 \mathbf{I} + \sum_{j \neq k} E\left[\mathbf{H}_k^* \mathbf{H}_k^T\right] \tag{4.2}$$

where σ_w^2 is the noise power.
Finally we can set the combiner weights by means of the following relation

$$\mathbf{U}_k = \alpha \mathbf{\Psi}_k^{-1} \mathbf{H}_k^H \tag{4.3}$$

where α is a constant that does not affect the SINR.

4.3 Minimum Mean-Square Error

Using a stream-by-stream optimization, we define the mean-square error (MSE) w.r.t. each stream of each user as

$$\begin{aligned} \eta_k^l &= E\left[\left|\widetilde{s}_k^l - s_k^l\right|^2\right] \\ &= 1 + \left(\mathbf{u}_k^l\right)^H \left(\mathbf{A}_k^l \mathbf{B}_k^l\right) \mathbf{u}_k^l - \left(\mathbf{u}_k^l\right)^H \mathbf{h}_k^l - \left(\mathbf{h}_k^l\right)^H \mathbf{u}_k^l \end{aligned} \tag{4.4}$$

where

$$\mathbf{A}_k^l = \mathbf{H}_{k,k} \mathbf{v}_k^l \left(\mathbf{v}_k^l\right)^H \left(\mathbf{H}_{k,k}\right)^H \tag{4.5}$$

$$\mathbf{B}_k^l = \left(\mathbf{\Xi}_{(k,l)} + \sum_{\forall (j,n) \neq (k,l)} \mathbf{H}_{k,j} \mathbf{v}_j^n \left(\mathbf{v}_j^n\right)^H \left(\mathbf{H}_{k,j}\right)^H \right), \tag{4.6}$$

are the terms representing, respectively, the signal and the noise plus interference statistical power, and

$$\mathbf{h}_k^l = \mathbf{H}_{k,k} \mathbf{v}_k^l. \tag{4.7}$$

The combiner vector $\mathbf{u}_k^l$ minimizing (4.4) is given by

$$\mathbf{u}_k^l = \frac{\left(\mathbf{A}_k^l + \mathbf{B}_k^l\right)^{-1} \mathbf{h}_k^l}{\left\| \left(\mathbf{A}_k^l + \mathbf{B}_k^l\right)^{-1} \mathbf{h}_k^l \right\|_F^2}. \tag{4.8}$$

To reduce its computational complexity in practical situations (4.8) can be implemented as a sparse filter [17], without a relevant loss of performance.

Remark

In [18, Sect. 8.3.3, pag. 359] it is shown that the maximum-SINR receiver also minimizes the minimum mean-square error (MMSE). Receivers of Sections 4.2 and 4.3 can be considered therefore equivalent unless a scaling factor. This aspect has been confirmed also from simulations performed.

Chapter 5

Beamformer design methods

5.1 Multiuser Eigenmode Transmission

The multiuser eigenmode transmission (MET) is a linear beamformer design technique based on block diagonalization (BD), that achieve interference suppression with a zero-forcing condition on the beamforming matrix.
Indeed, MET uses a combiner to select a sub-set of the eigenmodes of a given user, and a beamformer in order to guarantee orthogonality between the different users, resulting in a block diagonal channel matrix, meaning that no interference occurs between different users.
In this section we will cover the beamformer design, as first introduced in [19] and later improved in [20], togheter with two power allocation strategies. The classical SPC and a per-antenna power constraint (PAPC).

Considering our system model, the channel of user k can be decomposed using the singular-value decomposition (SVD) as $\mathbf{H}_k = \mathbf{Q}_k \mathbf{\Sigma}_k \mathbf{R}_k^H$, with the convention that singular-values in $\mathbf{\Sigma}_k$ are arranged so that the ones associated to user k appear in the leftmost d colums. The combiner of user k is a linear detector given by the Hermitian transposition of the leftmost d columns of $\mathbf{Q}_k$, i.e. $\mathbf{U}_k = \mathbf{Q}_{k,[1:d]}^H$, hence the cascade of the channel and the combiner gives

$$\boldsymbol{T}_k = \mathbf{U}_k^H \mathbf{H}_k = \left[\Sigma_{k,1}\mathbf{v}_{k,1}, \cdots, \Sigma_{k,d}\mathbf{v}_{k,d}\right]^H. \tag{5.1}$$

To avoid inter-user interference, conditions (3.19) must be satisfied, that is equivalent to say that $\mathbf{V}_k$ must lie in the null space of

$$\widetilde{\mathbf{H}}_k = \left[\boldsymbol{T}_1^H \ \cdots \ \boldsymbol{T}_{k-1}^H \ \boldsymbol{T}_{k+1}^H \ \cdots \ \boldsymbol{T}_K^H\right]^H. \tag{5.2}$$

To allocate at least one data stream per user, we see that (5.2) should not have a full rank, or equivalently it should be

$$d(K-1) < M. \tag{5.3}$$

Applying the SVD to matrix $\widetilde{\mathbf{H}}_k$ we get

$$\widetilde{\mathbf{H}}_k = \widetilde{\mathbf{Q}}_k \widetilde{\mathbf{\Sigma}}_k \left[\widetilde{\mathbf{R}}_k^{(1)} \ \widetilde{\mathbf{R}}_k^{(0)}\right]^H \tag{5.4}$$

where $\widetilde{\mathbf{R}}_k^{(0)}$ and $\widetilde{\mathbf{R}}_k^{(1)}$ holds the eigenvectors associated with the null and non-null singular values, respectively. Now we understand that to achieve interference alignment at receiver, that is verify (3.19), we can set

$$\mathbf{V}_k = \widetilde{\mathbf{R}}_k^{(0)} \mathbf{C}_k \mathbf{W}_k^{1/2}, \tag{5.5}$$

with $\mathbf{C}_k$ to be defined and $\mathbf{W}_k$ the diagonal matrix with allocated powers to eigenmodes. Correspondingly, we see that for any choice of $\mathbf{C}_k$ it is $\widetilde{\mathbf{H}}_k \mathbf{V}_k = \mathbf{0}$, since it is $\mathbf{T}_k \widetilde{\mathbf{R}}_j^{(0)} = \mathbf{0}$ for any $j \neq k$.
The received vector (3.13) is now simply

$$\mathbf{y}_k = \mathbf{H}_k \mathbf{V}_k \mathbf{s}_k + \mathbf{n}_k \tag{5.6}$$

since all interference from other users has been cancelled.
We consider now the product $\boldsymbol{T}_k \widetilde{\mathbf{R}}_k^{(0)}$, whose SVD gives

$$\boldsymbol{T}_k \widetilde{\mathbf{R}}_k^{(0)} = \bar{\mathbf{Q}}_k \begin{bmatrix} \bar{\boldsymbol{\Sigma}}_k & \mathbf{0} \end{bmatrix} \left[\bar{\mathbf{R}}_k^{(1)} \ \bar{\mathbf{R}}_k^{(0)} \right]^H. \tag{5.7}$$

where $\bar{\mathbf{R}}_k^{(0)}$ and $\bar{\mathbf{R}}_k^{(1)}$ are as in (5.4).
By setting $\mathbf{C}_k = \bar{\mathbf{R}}_k^{(1)}$, hence the signal subspace spanned by the non-null modes, we finally obtain a closed-form for the beamformer matrix of user k in the form

$$\mathbf{V}_k = \widetilde{\mathbf{R}}_k^{(0)} \bar{\mathbf{R}}_k^{(1)} \mathbf{W}_k^{1/2}. \tag{5.8}$$

We can now define the power allocation matrix. Recalling the equality

$$\|\mathbf{A}\|_F^2 = tr\left(\mathbf{A}\mathbf{A}^H\right), \tag{5.9}$$

the total amount of transmitted power is equal to

$$P_k = \|\mathbf{V}_k\|_F^2 = tr\left[\mathbf{V}_k \mathbf{V}_k^H\right] = tr[\mathbf{W}_k] \tag{5.10}$$

since by construction $\left\| \widetilde{\mathbf{R}}_k^{(0)} \bar{\mathbf{R}}_k^{(1)} \right\|_2^2 = 1$, while the signal power out of antenna m of user k is equal to

$$P_{k,m} = \sum_{j=1}^{d} |r_k^{(m,j)}|^2 w_k^{(j)} \tag{5.11}$$

where $r_k^{(m,j)}$ is the element (m,j) of the product $\widetilde{\mathbf{R}}_k^{(0)} \bar{\mathbf{R}}_k^{(1)}$ and $w_k^{(j)}$ the diagonal element j of $\mathbf{W}_k$.
In order to define the entries of $\mathbf{W}_k$, and considering a PAPC, we aim at maximizing the sum rate defined in (3.8) in the following way

$$\mathcal{R} = \max_{w_k^{(j)}} \sum_{k=1}^{K} \sum_{j=1}^{d} \log\left(1 + \Gamma\right) \tag{5.12}$$

$$\textit{subject to} \quad \begin{cases} w_j^{(k)} \geq 0 & k \in \{1, \cdots, K\}, j \in \{1, \cdots, d\} \\ \sum_{k=1}^{K} P_{k,m} \leq P_m^{MAX} & m = 1, \cdots, M \end{cases}$$

being $\sigma_j^{(k)^2}$ the j-th diagonal element of $\widetilde{\mathbf{\Sigma}}_k^2$ as from (5.7).
It is possible to solve this convex optimization by the interior point algorithm.
If instead we are interested in a SPC, the individual constraints for power allocation are replaced by a sum-power constraint

$$\sum_{k=1}^{K} P_k \leq \sum_{m=1}^{M} P_{k,m} = P_{MAX} \tag{5.13}$$

that can be solved using the Waterfilling algorithm (Appendix A). We highlight that since (5.12) is more restrictive that (5.13), its optimal value will result in equal or worst performance.

Performance results

We present now some results in Figure 5.1. MET proves to be a powerful and fast method to create an interference free subspace with few information about the system and without need to alternate the design procedure between Tx and Rx, since a closed-form solution is available. It complexity is then affected only by SVD operations, that have to be performed both at Tx and Rx, since no information exchange is required between different Tx users that could be eventually separate entities. Indeed, each Tx simply avoid to cause interference towards not-intended users while each Rx align its receiver subspace to the most favorable direction w.r.t. its own Tx. In general, this could not be the best strategy and we will see later in this work other way to reduce interference to other users and optimize the signal subspace at the same time.

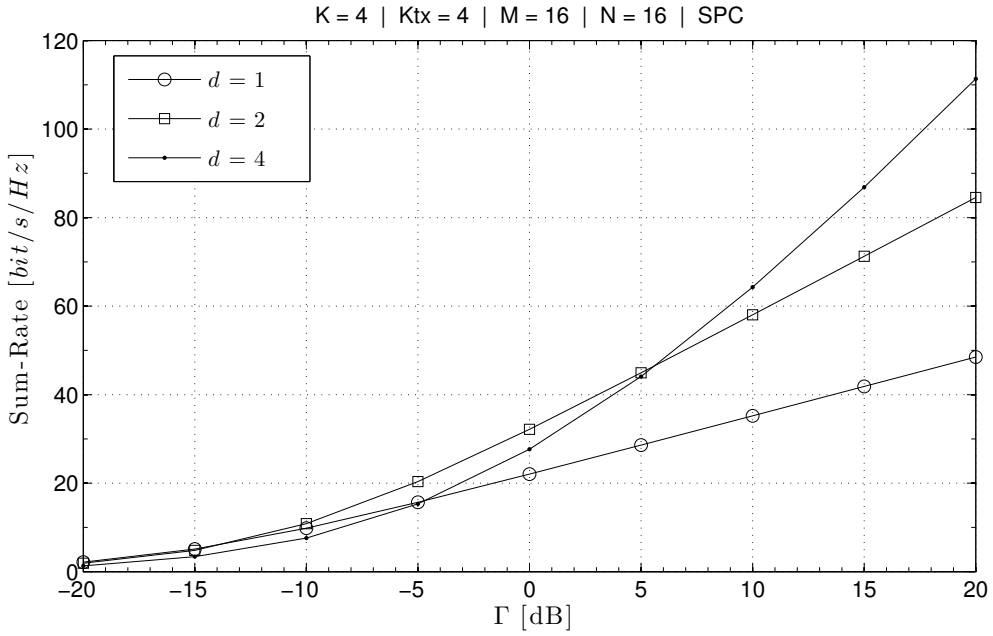

Figure 5.1: MET scheme with Rayleigh channel, effect of number of stream allocated for each user.

Since MET pursuits a zero forcing (ZF) solution, condition (5.3) needs to be verified in order to apply (5.5). Of course, relaxing the ZF condition would allow to apply MET

also in case where a perfect interference alignment is not possible. In particular, from (5.4) we can decide to take $\widetilde{\mathbf{R}}_k^{(0)}$ as the last d right singular vectors of $\widetilde{\mathbf{H}}_k$, even if not all associated with null-modes. However, this would result in very poor performance. In Fig. 5.2 we compare two cases in which we keep fixed all system parameters but the number of Tx and Rx antennas, so that in one case (5.3) is not fulfilled and residual interference strongly limits the achievable sum-rate. This because the design procedure takes care only on avoiding interference between different users and does not pay attention that the selected signal subspace is favorable for the transmission.

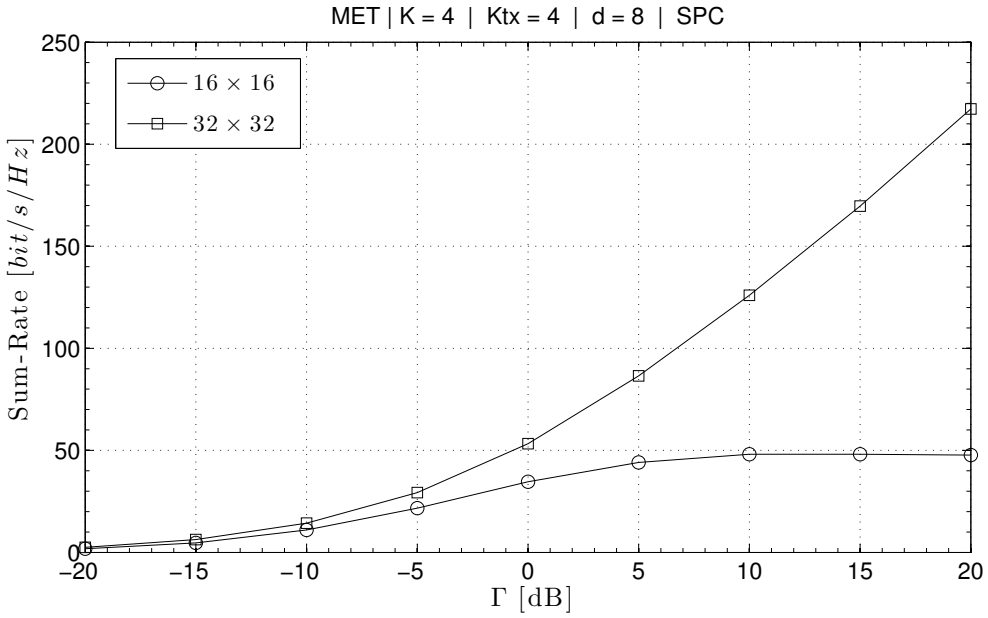

Figure 5.2: MET scheme with Rayleigh channel, effect of ZF condition.

Finally, no relevant differencies has been noticed between the downlink and the point-to-point case.

5.2 Minimum Interference-plus-Noise Leakage

In [21], the optimization problem is minimization of interference-plus-noise leakage (INL) caused by both user belonging to the system and interfering users that do not participate to the coordinated set of nodes, and thus referred as *uncoordinated interference*, so that we can overlap our coordinated interference to such coloured noise. This represents somehow a generalization of classical IA, where the noise is assumed white and all interferers participate to the alignment process.

For each user, we seek a subspace for which the interference cause by other transmission is minimum, and denote its orthonormal basis with $\mathbf{\Phi}_k$.

We can therefore use $\mathbf{\Phi}_k$ to project the received signal into the useful space, removing what is liying outside, and then a linear filter $\mathbf{G}_k$ to suppress intra-stream interference, so that our receiver filter will have the form $\mathbf{U}_k = \mathbf{G}_k\mathbf{\Phi}_k$.

As in previous cases, we start by defining a cost function to represent our INL as follows

$$\mathcal{I}_{INL} = \sum_{k=1}^{K} E\left[\left\|\mathbf{\Phi}_k^H\left(\sum_{\ell\neq k}\mathbf{H}_{k,\ell}\mathbf{V}_\ell + \mathbf{n}_\ell\right)\right\|_2^2\right] \tag{5.14}$$

where the expression inside brachet is the term (3.13) that takes into account the interference and noise affecting the useful signal.
Expanding the expectation and considering assumptions in (3.1), (5.14) becomes

$$\mathcal{I}_{INL} = \sum_{k=1}^{K}\sum_{\ell\neq k}\left\|\mathbf{\Phi}_k^H\mathbf{H}_{k,\ell}\mathbf{V}_\ell\right\|_2^2 + tr\left(\mathbf{\Phi}_k^H\mathbf{\Xi}_k\mathbf{\Phi}_k\right) \tag{5.15}$$

We can now write our objective function as

$$\begin{aligned} &\textit{minimize} && \mathcal{I}_{INL} && (5.16)\\ &\textit{subject to} && \mathbf{V}_\ell^H\mathbf{V}_\ell = \frac{P_\ell}{d}\mathbf{I}, \ell\in\{1,\cdots,K\} && (5.17)\\ & && \mathbf{\Phi}_k^H\mathbf{\Phi}_k = \mathbf{I}, k\in\{1,\cdots,K\} && (5.18)\end{aligned}$$

where (5.17) takes into account the power constraint of each user as defined in (3.2). Again, using (5.9) we further expand $\mathcal{I}_{INL}$ in

$$\mathcal{I}_{INL} = \sum_{k=1}^{K}\sum_{\ell\neq k} tr\left[\mathbf{\Phi}_k^H\left(\mathbf{H}_{k,\ell}\mathbf{V}_\ell\mathbf{V}_\ell^H\mathbf{H}_{k,\ell}^H + \mathbf{\Xi}_k\right)\mathbf{\Phi}_k\right] \tag{5.19}$$

The optimization is performed in the following way. Beamformers and combiners are alternatively updated so that the first will transmit over the subspace where it creates less interference to other users, while the latter will adapt the receiver's subspace to the one that sees less interference from other users. In particular, after initialization of combiners, e.g. chosing from the left singular vector of the channel matrix, we can update the beamformer matrix with the following rule

$$\boldsymbol{V}_\ell^{opt} = \nu_{min}^d\left(\sum_{k\neq\ell}\mathbf{H}_{k,\ell}^H\mathbf{\Phi}_k\mathbf{\Phi}_k^H\mathbf{H}_{k,\ell}\right). \tag{5.20}$$

where we recall $\nu_{min}^d(\mathbf{A})$ is the matrix whose column are the eigenvectors corresponding to the d smallest eigenvalues of matrix $\mathbf{A}$. Once we have updated the beamformers, we can use them to compute new values for combiners by means of the following

$$\mathbf{\Phi}_k^{opt} = \nu_{min}^d\left(\mathbf{\Xi}_k + \sum_{\ell\neq k}\mathbf{H}_{k,\ell}\mathbf{V}_\ell\mathbf{V}_\ell^H\mathbf{H}_{k,\ell}^H\right). \tag{5.21}$$

The two relations are then alternatively applied until convergency is reached.

Performance results

INL is a very light and fast algorithm and it does not require any knowledge a part from the cascade of beamformers/combiners with the cross channels, that can however easily collected by means of pilot sequence transmitted from Tx to Rx and back again. Every user can apply the update rule on its own and no information exchange is needed. Simulations show that INL behave quite well in situations where a ZF solution exists, but far from the performace offered by MET scheme, as can be seen in Fig. 5.3. In this situation, the convergency of the algorithm is really fast where ZF is possible while it need hundreds of iteration for more complex systems. A possible factor affecting performance could be the fact that while with MET the receivers were fixed to the leftmost singular vectors of the direct channel, so taking advantage from the best channel gains, in this case the Rx update rule can bring the receiver subspace on a shadowed alignment, even if with no interference.
However, if we test it in situations where perfect IA is not possible, we found that INL still gives good results with a relatively low computational cost at least for low SNR. At high SNR, we found that the residual interference becomes comparable to the noise power and therefore the sum-rate reaches asymptotically a maximum value, that depends on the number of iterations. The iterative approach becomes therefore relevant at high SNR and when ZF is not possible, as can be seen in Fig. 5.4.
Finally, in Fig. 5.5, we note that in the downlink case, so when the cross-channels are actually equal to the direct channel, the performance of INL are far lower than for the PP case.

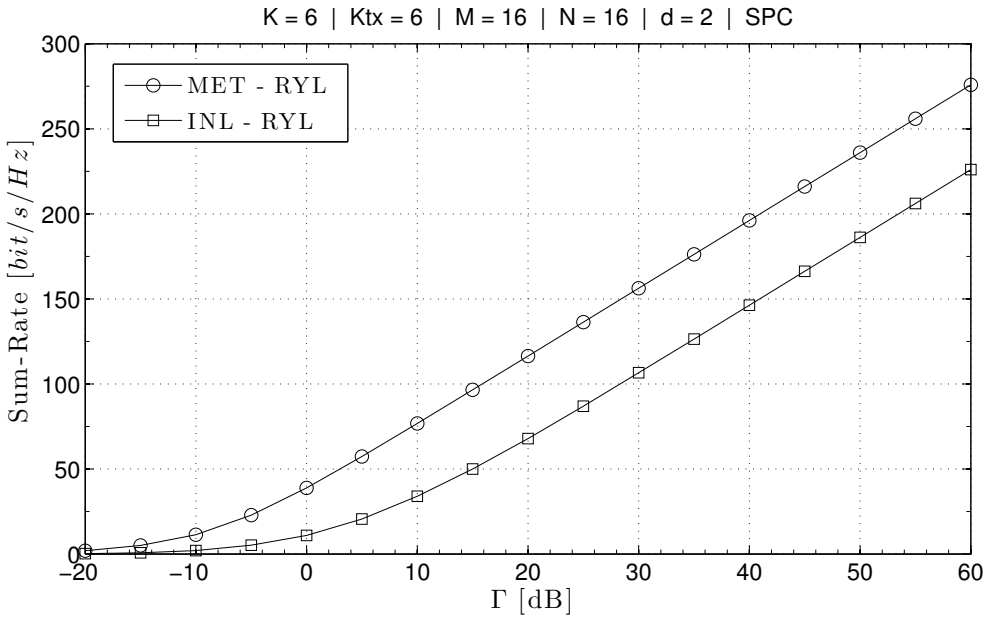

Figure 5.3: Comparison between INL and MET scheme considering a Rayleigh channel.

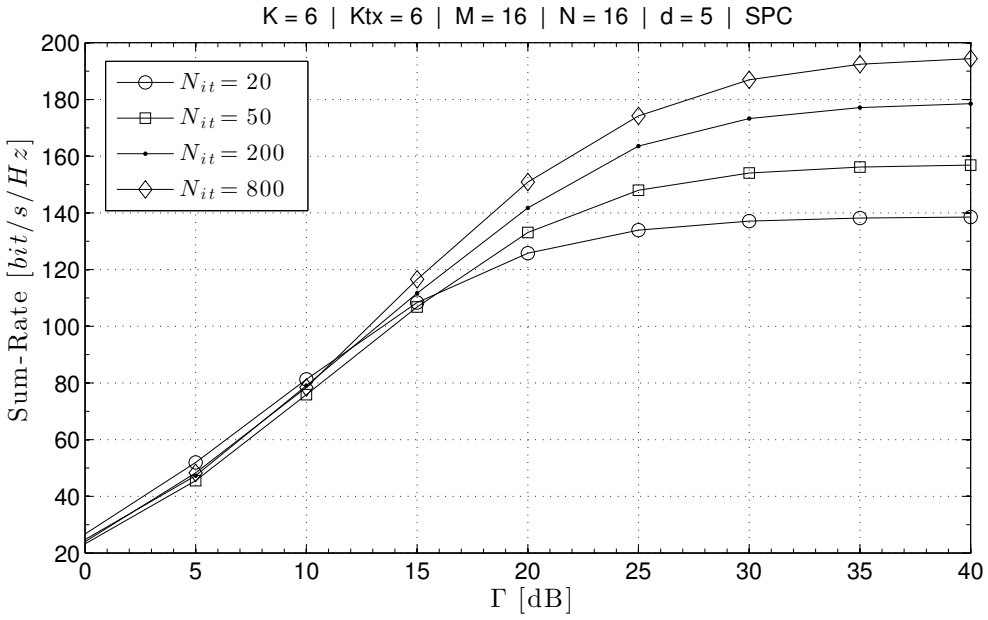

Figure 5.4: Effect of iterations for the INL scheme.

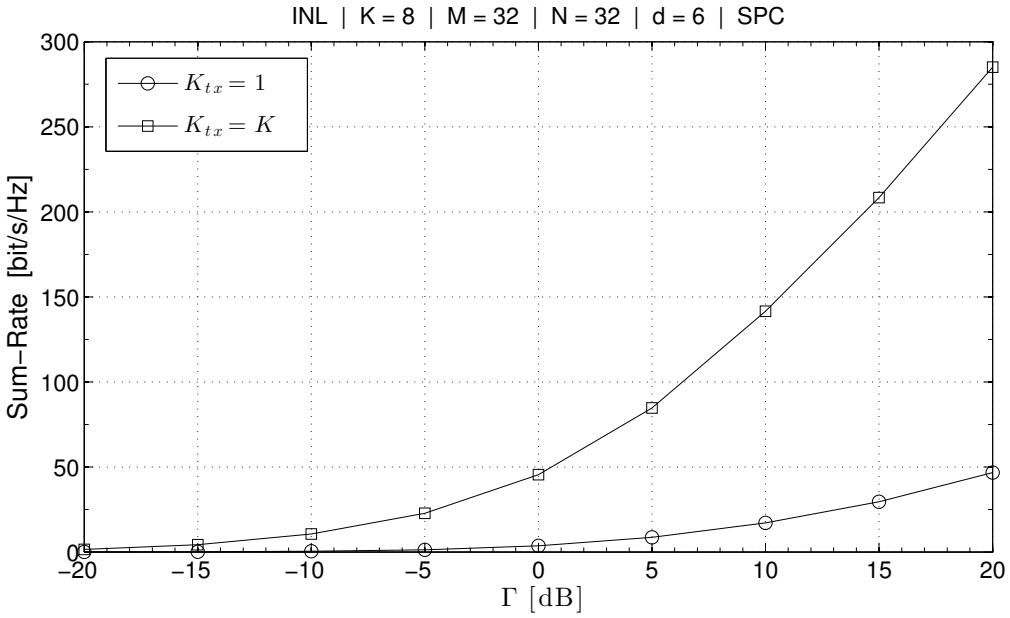

Figure 5.5: Comparison between the downlink and the point-to-point case with Rayleigh channel.

5.3 Maximum SINR

We have already shown a simple method for IA in Section 3.2, where channel reciprocity was used to update beamformers and combiners applying the same rule by simply switching the transmission direction. In [13] it is presented an evolution of such algorithm where the target is to maximize the SINR for each user instead of simply

avoiding interference. In fact, INL seeks to create an interference free subspace of the required number of dimensions but, in general, it makes no attempt to maximize the desired signal power within the selected subspace. Indeed, in the algorithms presented in Sections 5.1 and 5.2, the direct channel, $\mathbf{H}_{k,k}$, does not participate in the interference suppression procedure, resulting possibly in bad subspace choices as pointed out in Section 3.2. To take into account this last aspect, the new update rule will be the MMSE of (4.8). The steps to follow are listed in Algorithm 1. We recall that this procedure is based on the assumption that the channel can be reversed by setting $\overleftarrow{\mathbf{H}}_k = \mathbf{H}_k^H$, where the arrow state that we are considering the channel that goes from te receiver to the transmitter. Even if this assuption allows an easier implementation of the algorithm and makes possible to run it entirely at the transmitter side, it should be verified case by case. As already explained in Section 3.2, on the transmitter side, if signals from Rx users are received along a certain direction, transmitting on that direction will affect in the same way the signal received by Rx users. For that reason, aligning the beamformer over the highest SINR dimension involves that transmitting on that direction will reduce interference and maximize signal power at the same time.

Algorithm 1 Max-SINR algorithm

1: **Initialization:**
2: Start with arbitrary precoding matrices $\mathbf{V}_k$, with linearly independent column vectors.
3: **while** $\mathbf{u}_k^l(t), \mathbf{v}_k^l(t)$ *reach convergency* **do**
4: **for all** $k \in \{1, \cdots, K\}$ and $l \in \{1, \cdots, d\}$ **do**
5: Update receive combining vectors U_k with (4.3)
6: Reverse the communication direction ($\overleftarrow{\mathbf{H}}_k = \mathbf{H}_k^H$) and use the receive combining vectors as beamformers: $\overleftarrow{\mathbf{V}}_k = \mathbf{U}_k$
7: Update receive combining vectors $\overleftarrow{\mathbf{U}}_k$ with (4.3)
8: Reverse the communication direction and use the receive combiner vectors as beamformer vectors: $\mathbf{V}_k = \overleftarrow{\mathbf{U}}_k$
9: **end**
10: **end**

Performance results

SINR maximization can appears a selfish strategy to employ in a cooperative network, but it is instead a very powerful approach thanks to the exploitaion of the simmetric property of the channel. The update rule for the receiver is in fact the most intuitive way to design a combiner, that is choosing the subspace with the highest SINR. In Figures 5.6 and 5.7 we see the behavior of the MAX-SINR approach compared to the INL scheme with different streams allocated among users. We see that the MAX-SINR method clearly outperforms the INL scheme, especially when the allocated streams overload the system.
Regarding the implementation aspects, we need few dozen more iteration than with INL, but since are not involved operation like SVD we still have an acceptable computational cost. The update process can also in this case be performed independently by each user since the same kind of knowledge of the SINR algorithm is required.

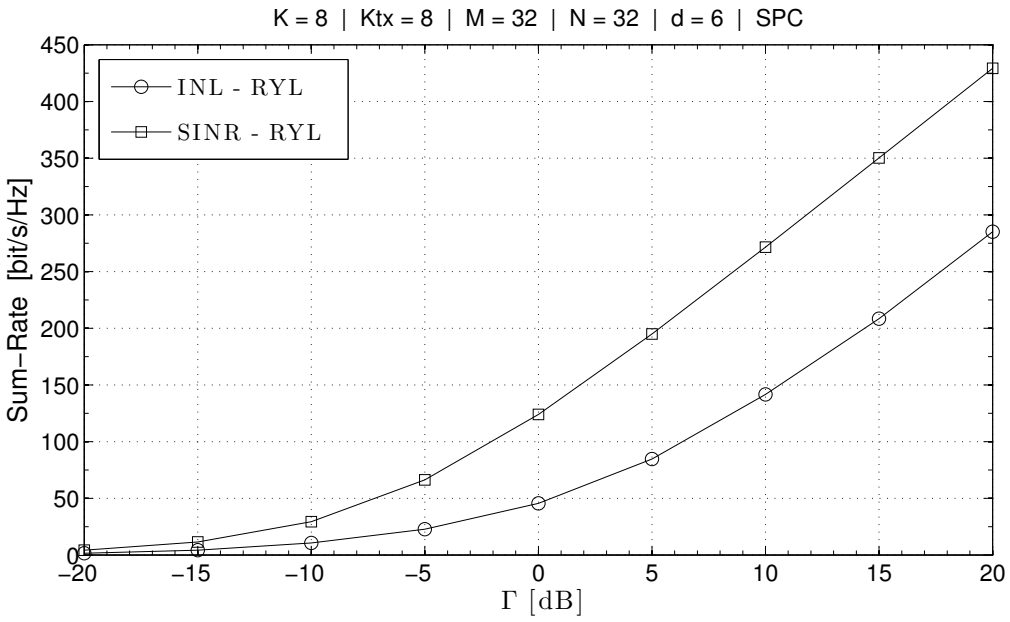

Figure 5.6: Comparison between INL and MAX-SINR performance with Rayleigh channel.

However, the channel reciprocity assumption may not be always valid and need to be verified, while the alternation between the direct and the inverse channel requires pilot sequences to be employed.

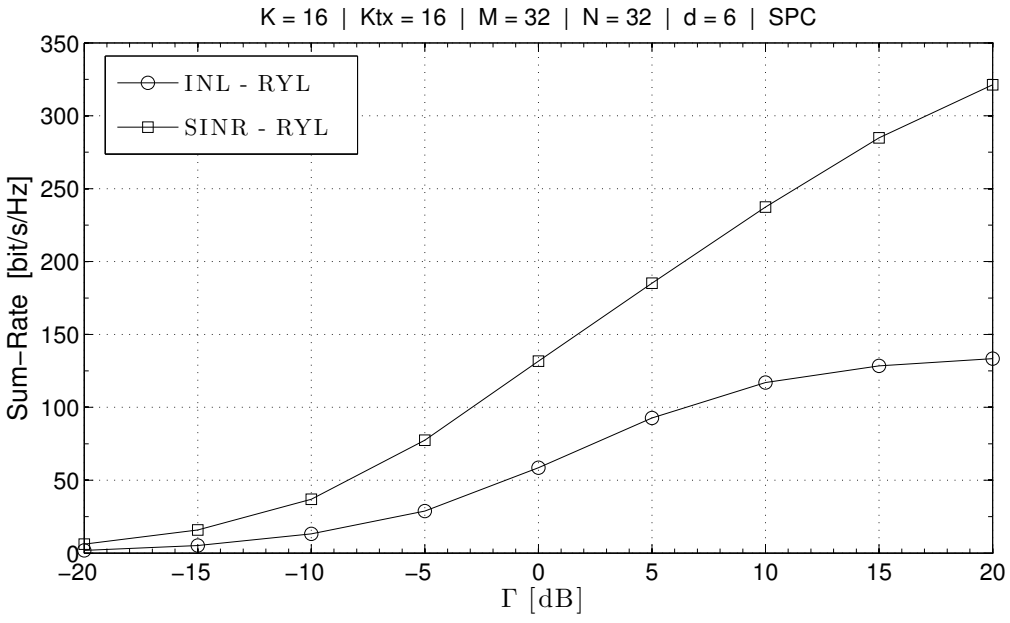

Figure 5.7: Comparison between INL and SINR performance with Rayleigh channel.

Also in this case, as can be seen in Fig. 5.8, we see a consistent performance gap between the downlink case and the point-to-point one. But differently to the INL algorithm, the difference appears only in network with many users, while it is absent for less crowded situations.

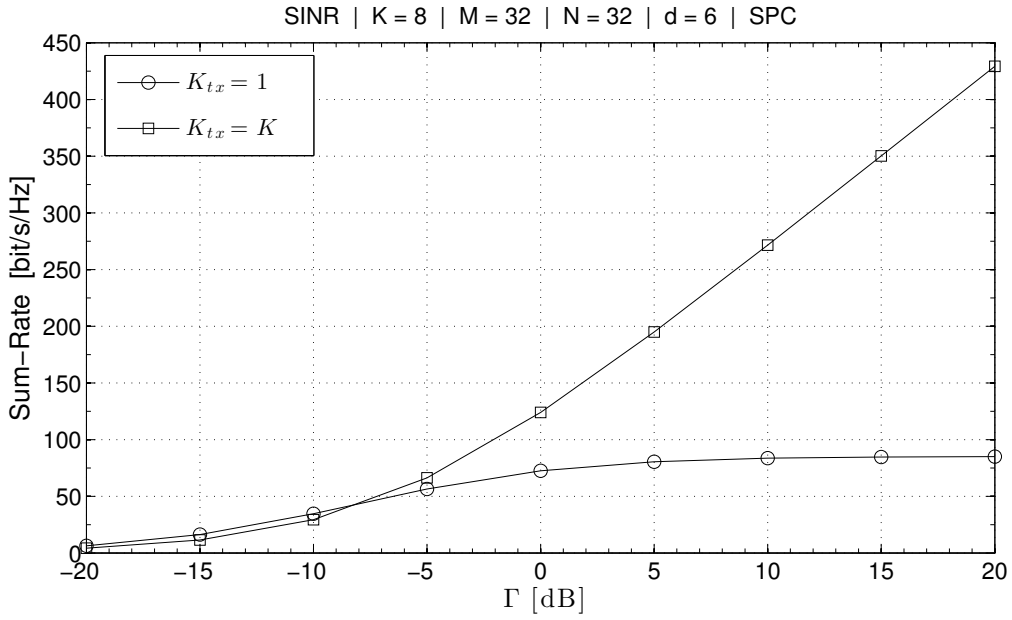

Figure 5.8: Comparison between the downlink and the point-to-point case with Rayleigh channel.

5.4 Weighted-Sum-Rate Maximization

This design approach, firstly described in [17] without the employment of weighting coefficients and then improved in [18], aim at maximizing the system sum-rate, i.e. the system rate given by the sum of the single user rates, defined as follow

$$\widetilde{\mathcal{R}}_{sum} = Kd \sum_{k=1}^{K} \sum_{l=1}^{d} w_k^l \mathcal{R}_k^l \tag{5.22}$$

where $\mathcal{R}_k^l$ is the achievable rate of the single stream (3.8) and w_k^l is the weight associated to the stream l of user k with the constraint $\sum_{\forall(k,l)} w_k^l = 1$.
The maximization problem is therefore

$$\max_{\mathbf{v}_k^l} \ \widetilde{\mathcal{R}}_{sum} \tag{5.23}$$

$$s.t. \ \|\mathbf{v}_k^l\|_2^2 = 1$$

For the beamformer desing it is made the assumption that each receiver makes use of a virtual combiner, despite of the actual implementation used. This will make possible to design the beamformer entirely at the transmitter side, without the need to alternate the design between transmitter and receiver. Such virtual combiner is a MMSE linear filter, whose design criterion has been described in Section 4.3.
For a given weight $\{w_k^l\}$, the Lagrangian optimization of (5.23) yield the following condition for the beamformer design:

$$\widetilde{\mathbf{\Upsilon}}_k^l \mathbf{v}_k^l \ = \ \widetilde{\lambda}_k^l \mathbf{v}_k^l \quad \forall(k,l) \tag{5.24}$$

where $\widetilde{\lambda}_k^l$ is the Lagrangian multiplier.

By introducing the following quantities

$$\gamma_j^n = \frac{1}{\left[\left(\mathbf{u}_j^n\right)^H \boldsymbol{\Xi}_{(k,l)} \mathbf{u}_j^n\right]} \tag{5.25}$$

$$\mathbf{B}_{(k,l)}^{(j,n)} = \gamma_j^n \left(\mathbf{H}_{j,k}\right)^H \mathbf{u}_j^n \left(\mathbf{u}_j^n\right)^H \mathbf{H}_{j,k}, \tag{5.26}$$

$$A_{(k,l)}^{(j,n)} = 1 + \gamma_j^n \sum_{\forall (j,q) \neq (k,l)} \left| \left(\mathbf{u}_j^n\right)^H \mathbf{H}_{j,i} \mathbf{v}_i^q \right|^2, \tag{5.27}$$

$$C_{(k,l)}^{(j,n)} = 1 + \gamma_j^n \sum_{\substack{\forall (i,q) \neq (k,l) \\ \forall (i,q) \neq (j,n)}} \left| \left(\mathbf{u}_j^n\right)^H \mathbf{H}_{j,i} \mathbf{v}_i^q \right|^2, \tag{5.28}$$

$$\bar{\mathbf{B}}_{(k,l)}^{(j,n)} = \frac{\mathbf{B}_{(k,l)}^{(j,n)}}{A_{(k,l)}^{(j,n)}}, \tag{5.29}$$

$$\widetilde{\mathbf{B}}_{(k,l)}^{(j,n)} = \frac{\mathbf{B}_{(k,l)}^{(j,n)}}{C_{(k,l)}^{(j,n)}}, \tag{5.30}$$

$\widetilde{\boldsymbol{\Upsilon}}_k^l$ can be expressed as

$$\widetilde{\boldsymbol{\Upsilon}}_k^l = \sum_{\forall (j,n)} \left\{ \frac{w_j^n \bar{\mathbf{B}}_{(k,l)}^{(j,n)}}{\left[1 + \left(\mathbf{v}_k^l\right)^H \bar{\mathbf{B}}_{(k,l)}^{(j,n)} \mathbf{v}_k^l\right]} \right\} - \sum_{\forall (j,n) \neq (k,l)} \left\{ \frac{w_j^n \widetilde{\mathbf{B}}_{(k,l)}^{(j,n)}}{\left[1 + \left(\mathbf{v}_k^l\right)^H \widetilde{\mathbf{B}}_{(k,l)}^{(j,n)} \mathbf{v}_k^l\right]} \right\} \tag{5.31}$$

for $j \in \{1, \cdots, K\}$, $n \in \{1, \cdots, d\}$.
Although the condition in Eq. (5.24) is in the form of a standard eigenvalue problem, the matrix $\widetilde{\boldsymbol{\Upsilon}}_k^l$ depends on the set of precoders $\mathbf{v}_k^l$ and a closed-form solution for such a problem is not available. Therefore, iterative procedures emerge as the only way to find an optimal solution.
The use of weights for the rate control of each stream is a classical strategy to adapt each link to its maximum achievable capacity, in particular the following weight design is based on the sum-rate defined in (5.22).
First of all, we write (5.22) as

$$\widetilde{\mathcal{R}}_{sum} = Kd \sum_{p=1}^{Kd} w_p \mathcal{R}_p \tag{5.32}$$

being $w_p = w_k^l$ and $R_p = R_k^l$, defining $p = (l + (k-1)d)$.
The single weights are then defined w.r.t. the sum of all other user's rates in the following way

$$w_k = \frac{\mathcal{R}_k}{\sum_{j=1}^{Kd} \mathcal{R}_j} \tag{5.33}$$

It can be verified [1] that when it is $w_k = w_k^{EQ} = \frac{1}{Kd}$, i.e. when all users have the same weight, the sum-rate is minimum.

[1] By recalling the Holder's inequality

The weights update will work in the following way: initially for all users and all stream $w_k^l = \frac{1}{Kd}$. The transmitter, after the optimization procedure considering the virtual combiner, sends the intended data streams to user k, which is employing a matched or mismatched combiner w.r.t. the virtual one. The receiver will therefore compute a new value for its weight, based on the actual combiner implemented and on the beamformer (5.33).
In Algorithms 2 and 3, the pseudo code of the design procedure is presented. In particular, the first focus on the weight update process that optimize the results given by the second, where the design of beamformer is described.
In Algorithm 3, the loop performed over the SNR range plays an important role in the reserch of a good local maximum for the beamformer vectors as it attempts to track a local optimum as the SNR is incrementally increased from zero. In fact, as explained in [15], this is motivated by the observation that as the SNR tends to zero, the noise dominates the interference, so that the optimal beams V_k tends to the principal eigenvectors of the direct channel $\mathbf{H}_k^H \mathbf{H}_k$. Furthermore, as the SNR tends to infinity, the set of local optima correspond to ZF (interference aligned) solutions (which depend only on the cross-channel matrices). The set of beams that maximize the sum utility at high SNRs should therefore be close to a ZF solution where the beams aligned are as closely as possible to the low-SNR solution. This intuition is illustrated in Fig. 5.9, where, for illustrative purposes, it is assumed that the optimization problem is one-dimensional.

Algorithm 2 Alternation-free multi-stream iterative IA Algorithm

1: **procedure** AT TRANSMITTER SIDE
2: **Initialization:**
3: $w_k^l \leftarrow \frac{1}{Kd}$, $k = \{1, \cdots, K\}$ $l = \{1, \cdots, d\}$
4: **while** $\mathbf{u}_k^l(t), \mathbf{v}_k^l(t)$ *reach convergency* **do**
5: With the current value of w_k^l, apply Algorithm 3
6: Recalculate w_k^l from (5.33) using equalizers and beamformers found in Algorithm 3
7: **end**
8: *Transmit data using beamformers* $\mathbf{v}_k^l$
9: **procedure** AT RECEIVER SIDE
10: *Computes* $\mathbf{u}$ *according to the design criterion employed.*
11: *Recalculate* w_k^l *, from (5.33), using the actual combiner employed at Rx*

$$\sum_{k=1}^{Q} |c_k d_k|^2 \leq \left(\sum_{k=1}^{Q} |c_k|^p \right)^{1/p} \left(\sum_{k=1}^{Q} |d_k|^q \right)^{1/q}, \; s.t. \; \frac{1}{q} + \frac{1}{p} = 1$$

where c_k and d_k are any complex numbers. For $q = p = 2$, $d_k = 1$, $c_k = R_k$, $\forall k$, we obtain

$$\sum_{k=1}^{Kd} \mathcal{R}_k \leq \left(\sum_{k=1}^{Kd} \mathcal{R}_k^2 \right)^{1/2} (Kd)^{1/2} \tag{5.34}$$

$$\Rightarrow \frac{1}{Kd} \sum_{k=1}^{Kd} \mathcal{R}_k = \sum_{k=1}^{Kd} w_k^{EQ} \mathcal{R}_k \leq \frac{\sum_{k=1}^{Kd} \mathcal{R}_k^2}{\sum_{k=1}^{Kd} \mathcal{R}_k} = \sum_{k=1}^{Kd} w_k \mathcal{R}_k \tag{5.35}$$

Algorithm 3 Beamformer Design

procedure AT TRANSMITTER SIDE
    Let $\Omega(t)$ and $\Psi(t)$ be a multidimensional matrix recording, respectively, the current values for beamformer and combiner of all users
    Initialization:
    $t \leftarrow 0$
    $\mathbf{v}_k^l(0) \leftarrow \nu_{max}^1 \left(H_{k,k}^H H_{k,k}\right), \forall(k,l)$
    $\Omega(0) \leftarrow \{\{\mathbf{v}_1^1(0), \cdots, \mathbf{v}_1^d(0)\}, \cdots, \{\mathbf{v}_K^1(0), \cdots, \mathbf{v}_K^d(0)\}\}$
    $\Psi(0) \leftarrow \{\{\mathbf{u}_1^1(0), \cdots, \mathbf{u}_1^d(0)\}, \cdots, \{\mathbf{u}_K^1(0), \cdots, \mathbf{u}_K^d(0)\}\}$
    $\Gamma \leftarrow 0$
    while $\Gamma_t < \Gamma_{max}$ **do**
        while $\mathbf{u}_k^l(t), \mathbf{v}_k^l(t)$ *reach convergency* **do**
            $t \leftarrow t + 1$
            for all $k \in \{1, \cdots, K\}$ **do**
                for all $l \in \{1, \cdots, d\}$ **do**
                    Using $\Omega(t-1)$*, use (4.8) to determine* $\mathbf{u}_k^l$
                end for
            end for
            $\Psi(t) \leftarrow \Psi(t-1)$
            for all $k \in \{1, \cdots, K\}$ **do**
                for all $l \in \{1, \cdots, d\}$ **do**
                    if $k = 1$ && $l = 1$ **then**
                        Update $\Omega(t) = \Omega(t-1)$
                    end if
                    Using $\Psi(t)$ *and* $\Omega(t)$ *, apply (5.24)*
                    Update $\Omega(t)$ with the new values of $\mathbf{v}_k^l(t)$
                end for
            end for
        $\Gamma_{t+1} \leftarrow \Gamma_t + \Delta\Gamma_t$
    end while

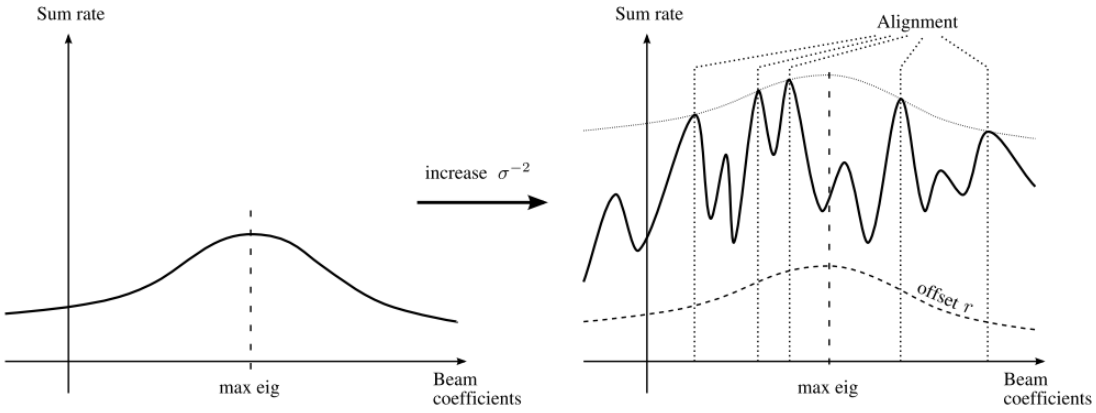

Figure 5.9: For low SNR (left), the optimal beamforming strategy is easily found and consists of using the principal eigenvectors of the Gramians of the direct channels. At high SNR (right), there are many local optimizers which depend only on the cross channels. The best aligned solution is the one with the highest high-SNR offset r, which depends only on the direct channels. We are therefore interested in finding aligned solutions that are close to the low-SNR optimal strategy.

Performance results

The simulations shows that this algorithm perform quite well and performances get close to MAX-SINR, at least for low values of SNR. However, it comes at a very high computational cost. We have seen that Eq. (5.24) needs an iterative procedure to be solved, while the beamformers and combiners design alternation needs about 800 iteration to converge, as shown in [18]. Moreover, we might wonder whether the optimization procedures proposed are actually valuable for practical application. We have mentioned that the iteration performed over different values of the SNR was a way to obtain beamformers that was optimum or near-optimum for both low and high noise levels, but it is in doubt the advantage of design beamformers that are suitable for tens of different dB values but valid only for a given channel realization at the price of repeating several times the design procedure. In the previous algorithms treated in this work, by initializing beamformers as the principal eigenvectors of the direct channel, we obtained good values at low SNR, i.e. less than $20dB$, with few iteration. The same holds for WSR, so that considering SNR in the design procedure is not always needed. Finally, we want to consider the effect of the weights strategy on the system sum-rate. In the paper, the author claims that the weights are needed to deal with mismatches of receiver combiners from the virtual combiner that is assumed at the transmitter, but it seems a very particular situation to have a system where receiver can implement different types of combiner. Moreover, when all the receivers are matched to the MMSE virtual one assumed for the beamformer design, no improvements are observed.

In Figure 5.10 it is reported an example of the performance achieved in the point-to-point configuration, while in Figure 5.11 the same results are shown for the downlink case. As in previous algorithms, when the transmitters belong to the same physical location, the overall throughput is affected from the high correlation between direct channel and cross-channels.

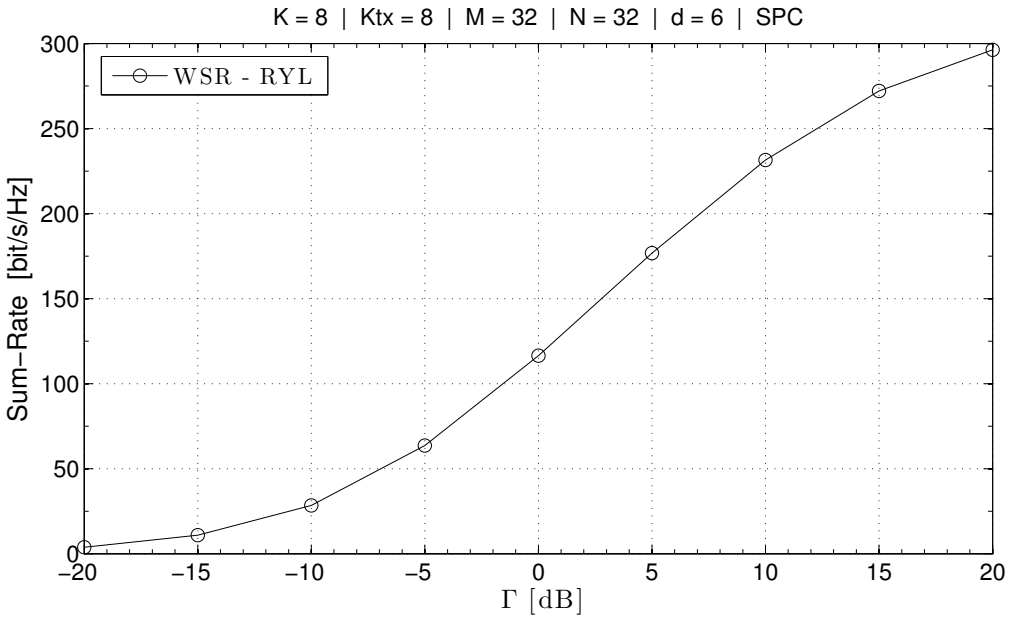

Figure 5.10: Performance of the WSR scheme in a PP scenario with Rayleigh channel

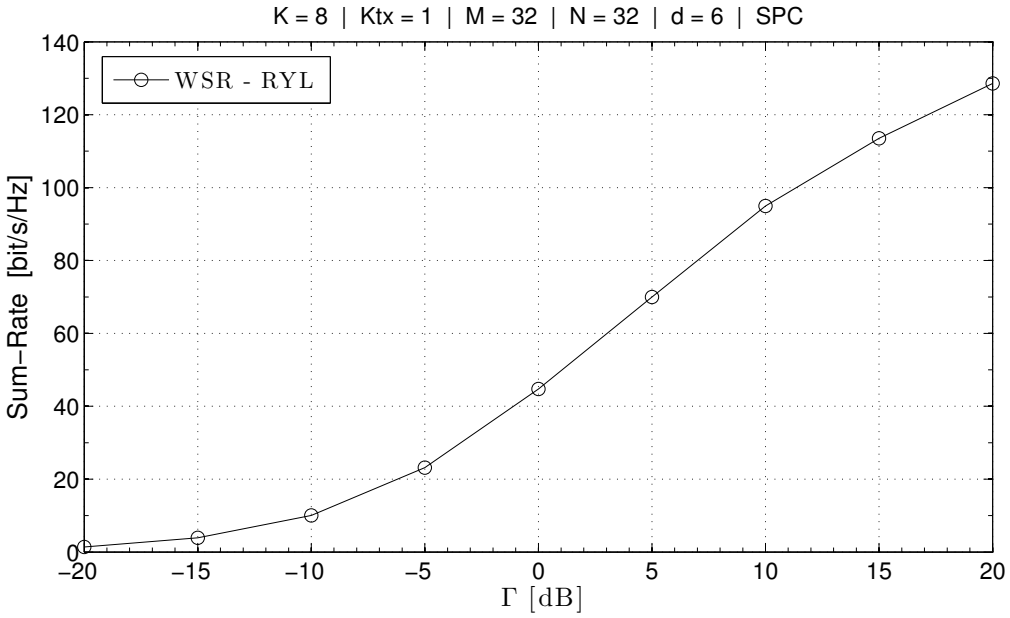

Figure 5.11: Performance of the WSR scheme in a DL scenario with Rayleigh channel

Chapter 6

Results

As we have seen in Section 2.2, the MMW channel is characterized by a high correlation between antennas, due mostly to the fact that signals propagates from Tx to Rx across few rays, three in our case, and with similar delay and angle of arrival (AoA). One of the consequences is a channel matrix where the diversity offered by the channel is limited. In particular, our channel matrix will have a constant rank, equal to the number of rays that reach the receiver, independently from the size of the antenna array. Under this point of view one could wonder what is then the advantage of increasing the number of antennas when the diversity provided will not be affected. The reason can be found by analysing the gain provided by its non-null modes. In fact, as can be seen from Fig. 6.1, we can note that the magnitude of the eigenvalues of our channel matrix is increasing together with the number of antennas composing the arrays.

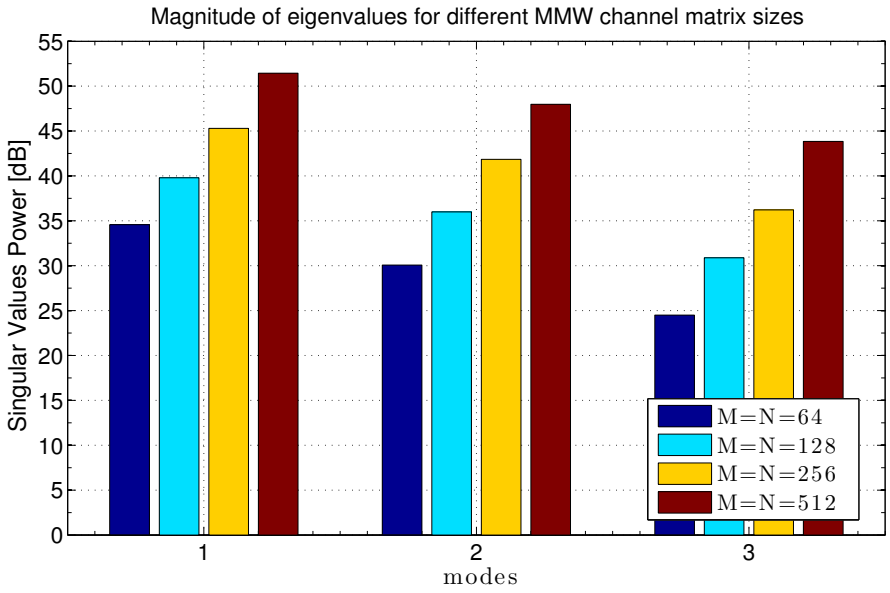

Figure 6.1: Magnitude of the eigenvalues of the MMW channel matrix for different array sizes.

Moreover, in Fig. 6.2, where is shown the same aspect over a classical Rayleigh fading channel, it is of interest to note how the magnitude of the eigenvalues remains constant among the modes and that this value is several decibels lower than the correspondent modes of the MMW channel. However, it would be wrong to think that the MMW channel has somehow advantages w.r.t. the classical Rayleigh fading. In fact, we have

shown only the first three modes, that are the only non-null modes for the MMW channel, but we should keep in mind that a Rayleigh fading channel matrix is always full rank and therefore has as many different modes as the number of antennas composing the arrays. For this reason, it is believed that it would be not fair to compare performance between the two different channels by assuming the same transmission rank, that in the MMW case is limited to the number of existing rays. Instead it is reasonable to compare the two channels with the higher number of modes that each can support.

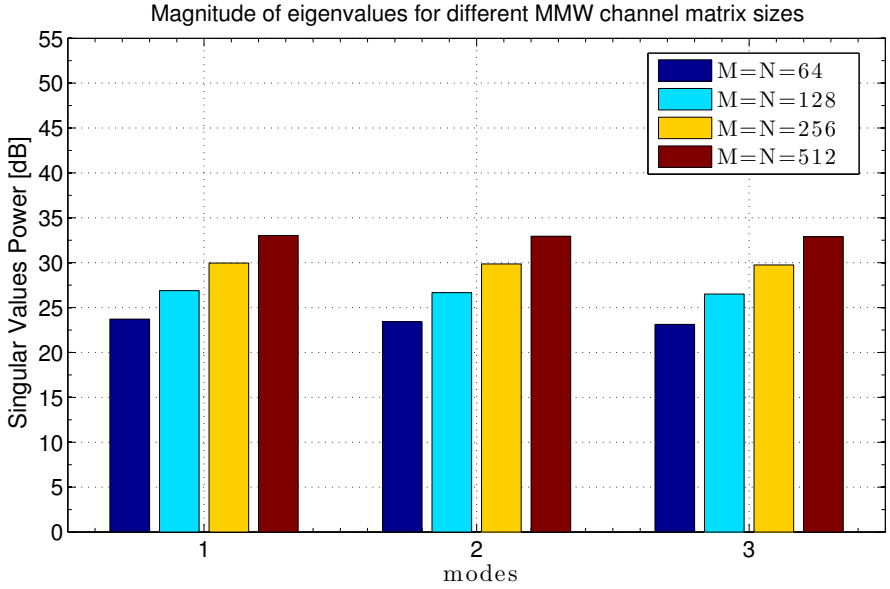

Figure 6.2: Magnitude of the eigenvalues of the Rayleigh channel matrix for different array sizes.

In Figures 6.3 and 6.4 it is compared the sum-rate achieved by the MET algorithm [20] over the two considered channel when, respectively, three and twenty modes are employed for the transmission and considering antenna arrays of $M = N = 256$ elements. Power allocation is performed by applying Water Filling, so that beamforming over the MMW channel is actually performend using the only three non-null modes. What happens is that with Rayleigh channel the sum-rate grows togheter with the signal subspace dimension, while the MMW channel available modes limit the maximum achievable sum-rate. Of course, using massive antenna arrays over the normal ultra high frequency (UHF) spectrum would mean having a huge array size that would not be suitable for portable devices. On the other hand, we have seen that the single modes are more powerful in the MMW, so that it slightly ouperforms the Rayleigh channel when the same number of modes are considered and the gap between them scale with the number of antennas composing the arrays since the growth rate of modes magnitude is higher for the MMW. We can therefore think that system at MMW could be more suitable for situation in which many users that don't require excessive bandwidth have to share the same channel.

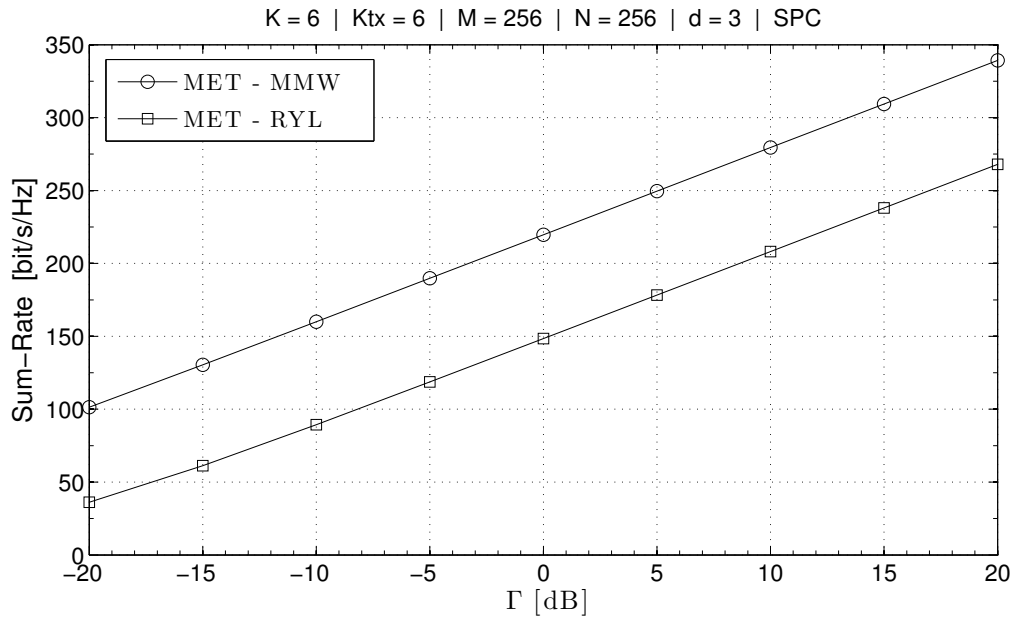

Figure 6.3: System sum-rate with MET scheme [20] over MMW and RYL channels, when three streams per user are considered.

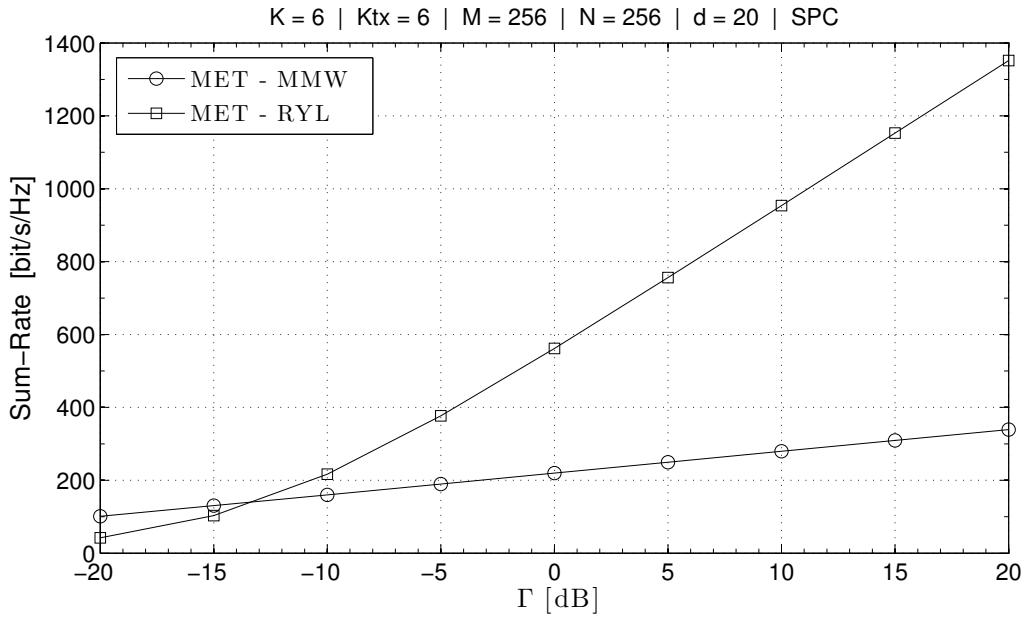

Figure 6.4: System sum-rate with MET scheme [20] over MMW and RYL channels, when twenty streams per user are considered.

The same results hold for the other algorithms, as can be seen from Figures 6.5 and 6.6, where the Rayleigh channel provides higher rates thanks to the diversity that can offer.

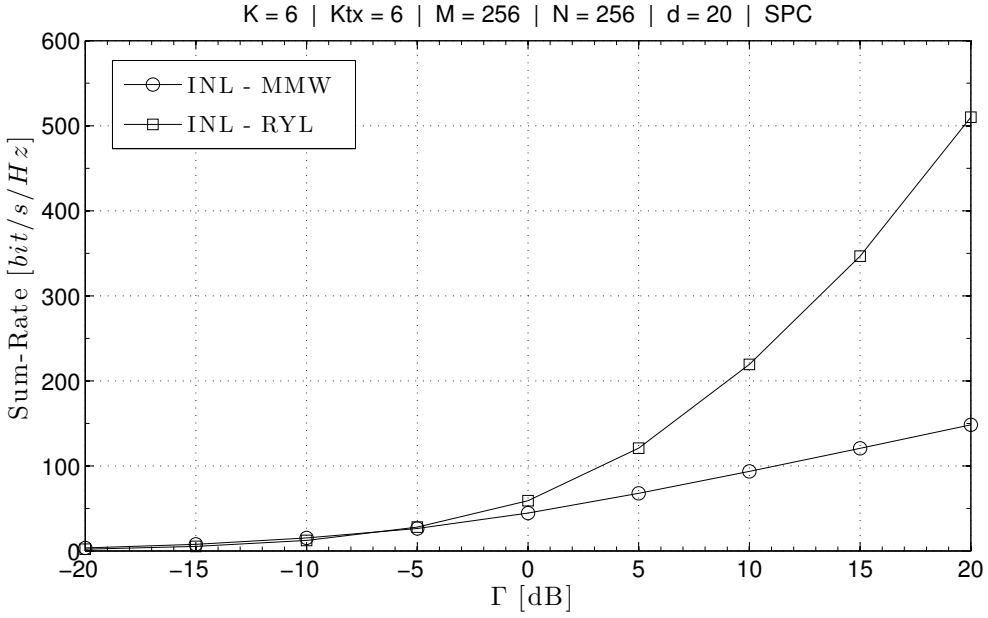

Figure 6.5: System sum-rate with INL scheme over MMW and RYL channels.

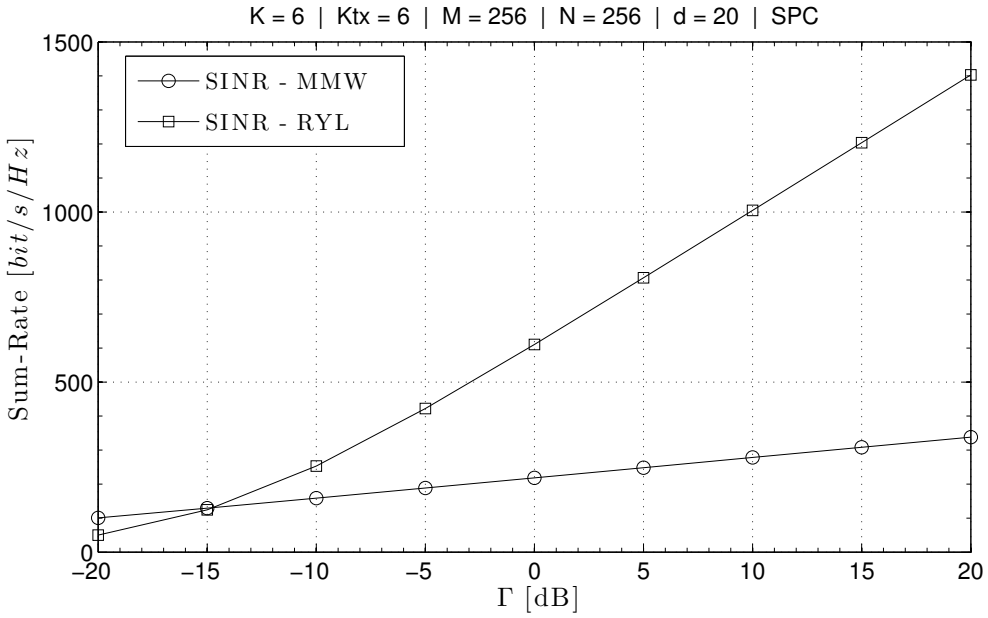

Figure 6.6: System sum-rate with SINR scheme over MMW and RYL channels.

Now that we have analysed pros and cons of the MMW channel, we can take a look over the behavior of the different algorithms considered and try to understand what strategies can better exploit its properties. In the following figures, all the method previously explained are compared in different system configurations and for antenna arrays of $M = N = 128$ elements. In Figures 6.7 and 6.8 we compare the difference

with the Rayleigh channel. In both scenarios the relative performances are similar and all methods but the INL one reach the same sum-rate. Indeed, we are in a very favourable situation, since the possibility of using a huge number of antennas compared to the transmission order implies a high order of degrees of freedom (DoF) in which align the interference components.

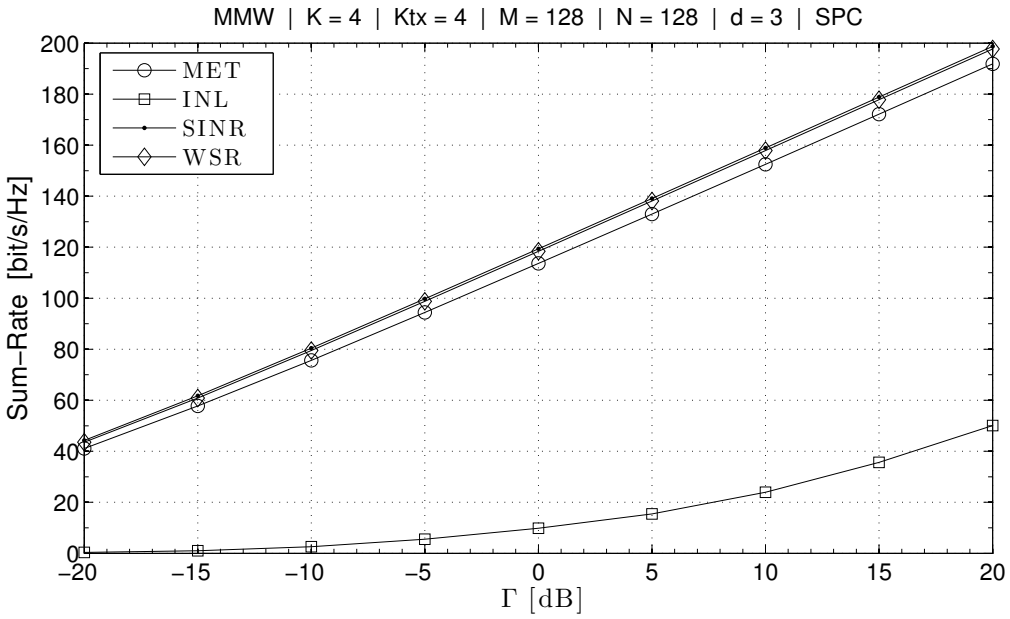

Figure 6.7: Sum-rate achieved by all considered algorithms with the MMW channel with a low number of users (four Tx/Rx pairs).

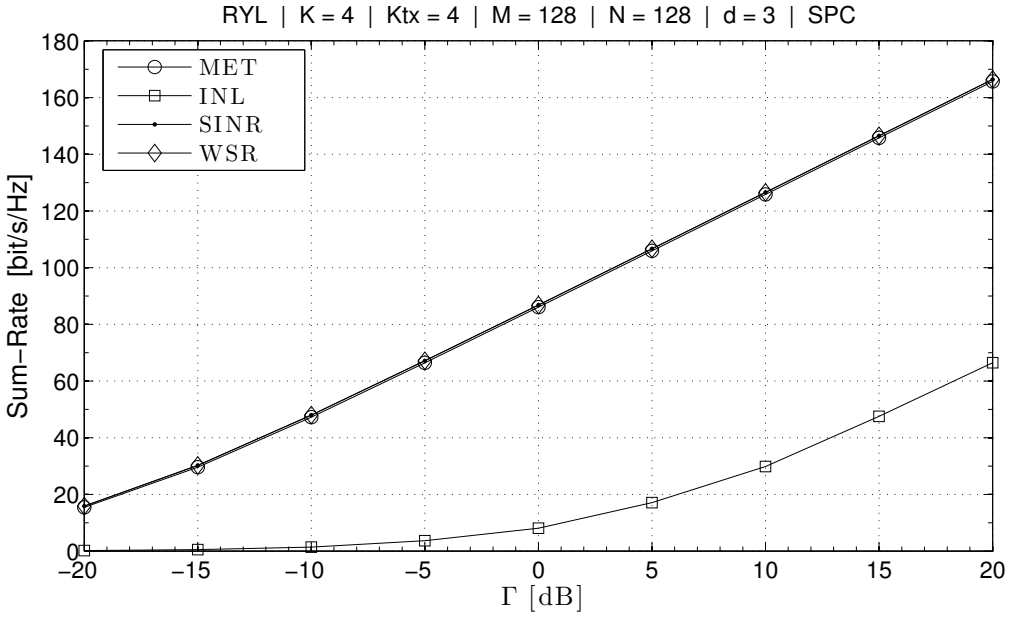

Figure 6.8: Sum-rate achieved by all considered algorithms with the RYL channel with a low number of users (four Tx/Rx pairs).

A different trend appears when the number of users increase. As can be seen from

Fig. 6.9, while MAX-SINR and WSR are able to withstand these conditions, MET suffers from the reduced available space in which accomondate every single user. As said before, this is probably due to the limited degrees of freedom offered by the MMW channel, that prevent to find enough space to accomodate signal and interferers in separate subspaces so in that particular situation the best approach would be to consider also the gain provided to the desidered signal instead of take care only to cancel interference.

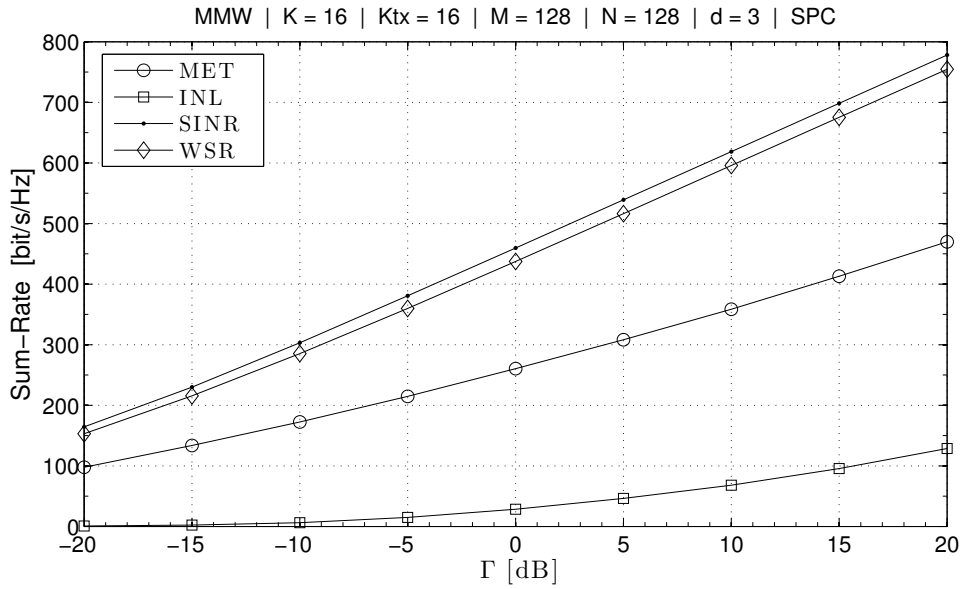

Figure 6.9: Sum-rate achieved by all considered algorithms with the MMW channel with a high number of users (sixteen Tx/Rx pairs).

To complete our results discussion, we show the behavior of the studied algorithms when a downlink scenario is considered. In Figure 6.10 we can compare the sum-rate achieved when the different transmitters share the same antenna array with the corresponding PP case shown in Figure 6.7.
As we can see, the MET algorithm does not changes remarkably its behavior between the two cases, like in the Rayleigh channel, but surprisingly also the MAX-SINR method is capable of mantain its performances with the DL case, differently from what seen in the Rayleigh fading case (Figure 5.8). The INL and the WSR algorithms, on the other hand, are annihilated by this situation. Focusing furthermore on the MET and MAX-SINR methods in the DL scenario, we have that in more crowded network, as reported in Figure 6.11, we see that performances are lightly affected if compared with the ones found in Figure 6.9. In particular, MET is even improving its performance (actually it has been originally designed for a DL scenario, differently from the others), while for the MAX-SINR algorithm we don't have the same performance gap as the one given by the Rayleigh scenario of Figure 5.8. This is indeed an interesting situation that can possibly represent an advantage of MMW channels.

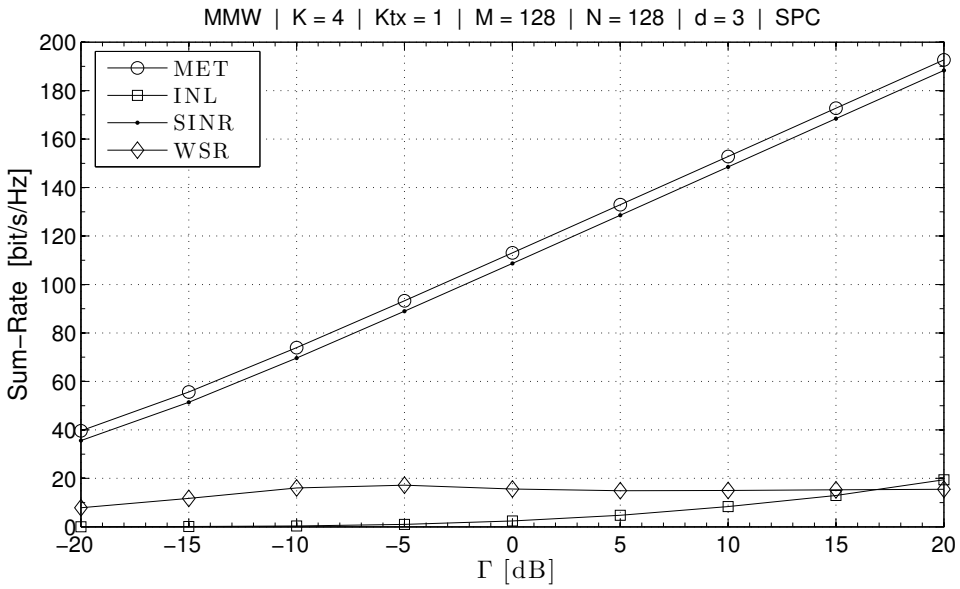

Figure 6.10: Sum-rate achieved by all considered algorithms with the MMW channel considering a downlink scenario.

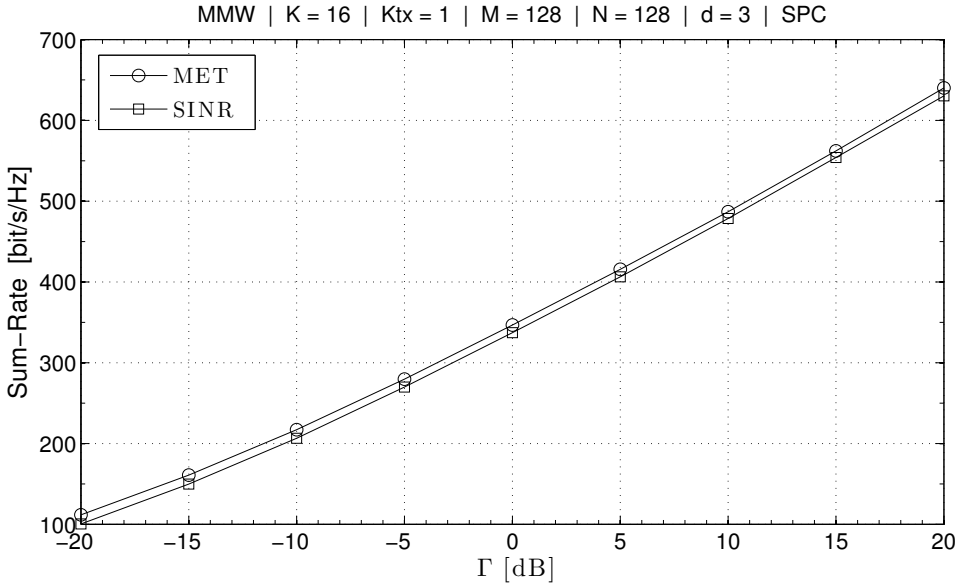

Figure 6.11: Downlink case for the MET and MAX-SINR algorithms in crowded situations (sixteen Tx/Rx pairs).

Chapter 7

Frequency Domain Equalization for Wideband Channels

For a transmission over frequency selective channels, it is proposed a FS iterative block decision feedback equalizer (FS-IBDFE) receiver that combines the advantages of FS equalization, non-linear processing and FD implementation. The improvements given by this receiver are: a) the extension of existing FD iterative equalization schemes considering a FS processing; b) the design of the FD equalizer coefficients minimizing the mean-square error at the detection point; and c) a simple equalizer design procedure where equalization coefficients are computed in closed form, without matrix inversions. As an example, performance of the proposed scheme is assessed in a Rayleigh fading channel and it is seen that the FS-IBDFE significantly outperforms the FS-linear equalizer (LE), the non-FS iterative block DFE (IBDFE) and the noise prediction FS FD equalizer (NP-FS-FDE).

7.1 Introduction

Transmission over broadband channels yields ISI, which can be addressed by various techniques at the receiver. The solution that minimizes the error probability is provided by a maximum likelihood sequence detector receiver [22], whose complexity grows exponentially with both the number of equivalent channel taps and the constellation size.

When equalization techniques are employed the complexity instead grows linearly with the number of receive filter taps. A further complexity reduction is achieved by performing equalization in the FD, by using a block-based transmission format (cyclic prefix or unique-word extended transmission) and applying discrete Fourier transform (DFT) on the received block [23]. Indeed, it has been shown that best performance are achieved by using non-linear equalization structures where filtering and detection are iterated [24]. On the other hand, FS receivers yield better performance in dispersive channels, as they prevent folding of the channel frequency response. They also allow a greater flexibility in the choice of the sampling phase. FD equalization of FS signals has been first proposed in [25] where however only LEs have been considered. Among other receiver structures, FS-LEs have been also used in [26], while noise prediction configurations are proposed in [27]. Since performance evaluation will be compared to the IBDFE of [28] and the NP-FS-FDE configuration of [27], a brief description of those schemes is given, respectively, in Appendix B and C.

7.2 Channel Model

We consider a transmission system where data symbols a_m, $m = 0, 1, \ldots$ are transmitted from a transmitter filter, having impulse response $g_{\text{tx}}(t)$, through a Rayleigh fading channel having impulse response $g_{ch}(t)$, for which we define the equivalent impulse response as

$$h_{\text{ch}}(t) = g_{\text{tx}} * g_{\text{ch}}(t), \tag{7.1}$$

with energy

$$E_{h_{\text{ch}}} = \int_{-\infty}^{\infty} |h_{\text{ch}}(t)|^2 dt. \tag{7.2}$$

At the receiver front-end, additive white gaussian noise (AWGN) with power spectral density (PSD) N_0 is added to the transmitted signal that is finally received by a filter with impulse response $g_{\text{rx}}(t)$. The cascade of the transmit, the channel and the receive filters will be denoted as

$$h(t) = g_{\text{tx}} * g_{ch} * g_{\text{rx}}(t). \tag{7.3}$$

The received signal is then sampled with a period T_s that represents the system time. In Fig. 7.1 it is reported the scheme of the channel model just introduced.

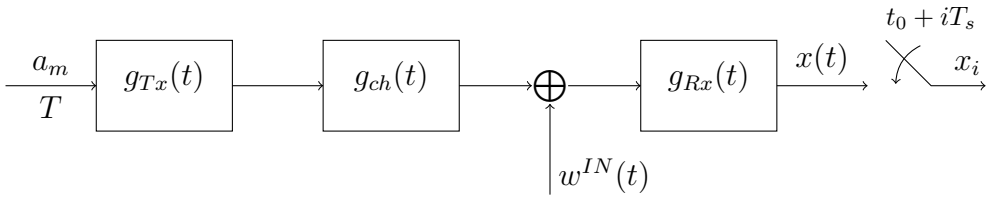

Figure 7.1: Channel scheme.

As can be seen from Fig. 7.2, where is reported the equivalent channel scheme at system time $T_s = T/2$, the signal after sampling at Rx can be written as

$$x_i = v_i + w_i = \sum_{k=0}^{N_h-1} h_k s_{i-k} + w_i \tag{7.4}$$

where, by a proper sampling phase, $h_i = h(iT/2)$, $i = 0, \ldots, N_{\text{h}} - 1$, and w_i is the noise term. In particular, w_i is obtained by filtering a complex value zero-mean AWGN $w_i^{(\text{IN})}$, having power spectral density N_0, with the receive filter having impulse response $\{g_i = g_{\text{rx}}(iT/2)\}$, with $i = 0, \ldots, N_{\text{g}} - 1$.
By further defining as

$$M_a = E\left[|a_m|^2\right] \tag{7.5}$$

the average power of the transmitted data sequence, the signal-to-noise ratio at the receiver front-end is equal to

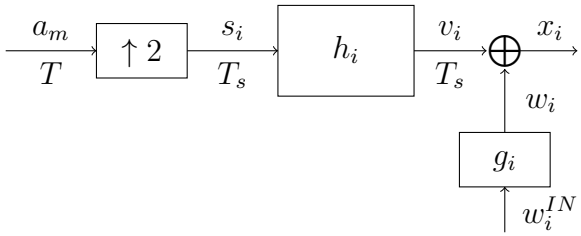

Figure 7.2: Equivalent channel scheme.

$$\Gamma = \frac{M_s}{N_0/T} = \frac{M_a E_{h_{ch}}}{T} \frac{1}{N_0/T} = \frac{M_a E_{h_{ch}}}{N_0}. \tag{7.6}$$

Notation:

In the following chapter, the DFT over $2P$ samples of a signal in the time domain (TD) u_i, $i = 0, \ldots, 2P-1$, is denoted by its corresponding upper case letter, and DFT and inverse discrete Fourier transform (IDFT) are defined, respectively, as

$$U_p = \sum_{k=0}^{2P-1} u_k e^{-j\frac{2\pi kp}{2P}}, \quad u_i = \frac{1}{2P} \sum_{k=0}^{2P-1} U_p e^{j\frac{2\pi ip}{2P}}, \tag{7.7}$$

where $j = \sqrt{-1}$, and $i, p = 0, 1, \ldots, 2P-1$. The real part of x is denoted as $\Re(x)$. The complex conjugate of x is denoted as x^* while the complex conjugate transpose of vector $\boldsymbol{v}$ is $\boldsymbol{v}^H$. $\lceil x \rceil$ denotes the ceiling of x.

7.3 System Model

Given a sequence of information bits, after encoding, interleaving and bit mapping, symbols a_m, $m = 0, 1, \ldots$, are transmitted at rate $1/T$, and the signal after the receive filter is sampled at rate $2/T$. Let s_i be the upsampled version of a_m, i.e.,

$$s_{2m} = a_m, \quad s_{2m+1} = 0 \tag{7.8}$$

for $m = 0, 1, \ldots$.

The equalization structures that will be presented in the following sections require a particular block transmission format, denoted *pseudo noise (PN)-extended transmission*, which both removes the interference between blocks [see (7.9)] and forces the convolution between data and equivalent channel impulse response to be circular, hence processing at the receiver can be easily implemented in the FD [24]. In particular, data symbols $\{d_m\}$ are organized into blocks of length M, and each block is extended with a fixed sequence of L symbols, for example a PN sequence $\{q_m\}$, $m = 0, \ldots, L-1$, which is assumed to be known at the receiver, providing blocks of size $P = M + L$. Therefore, signal $\{a_m\}$ of block ℓ can be written as $a_{m+\ell P} = d_{m+M\ell}$ for $m = 0, \ldots, M-1$ and $a_{m+\ell P} = q_{m-M}$ for $m = M, \ldots, P-1$, where the last L symbols are the PN sequence. An additional PN extension is required before the first data block. Note that if $1/T$

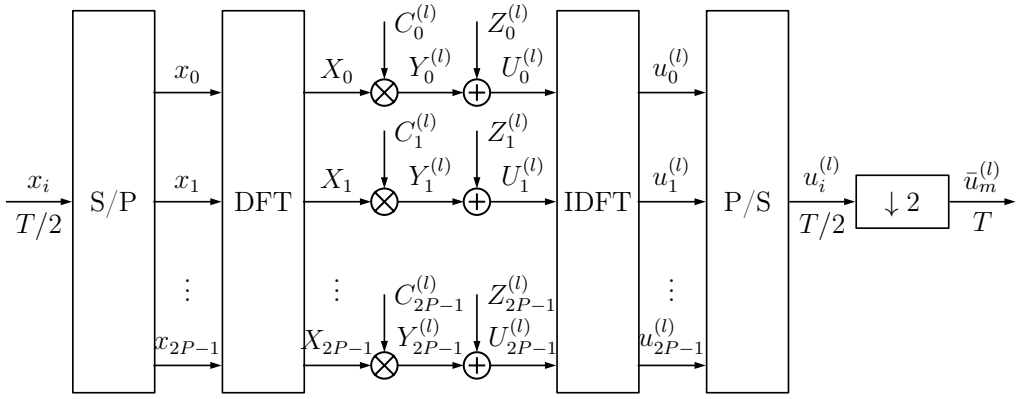

Figure 7.3: feedforward part of the FS-IBDFE operating at $T/2$.

remains the transmission rate, the symbol rate of a_m will be now $1/T' = (M/P)/T$, i.e., we are transmitting at a slower data rate. In the following we will assume that

$$L \geq \lceil (N_{\rm h} - 1)/2 \rceil, \tag{7.9}$$

so that by taking blocks of x_i of size $2P$, in each block the first $2M$ samples are not affected by interference due to adjacent blocks. Therefore, without restrictions, we focus on the transmission/reception of the first block, i.e., for x_i with $i = 0, \ldots, 2P-1$, and we set the block index to zero, $\ell = 0$.

7.4 Fractionally Spaced IBDFE

The FS-IBDFE scheme, operating on blocks of the received signal, is shown in Fig.s 7.3 and 7.4. The scheme performs iterated operations on each $2P$-size block of the received signal [28]. We denote with $l = 0, 1, \ldots, N_I - 1$, the iteration number. The equalizer includes two parts: 1) the feedforward (FF) filter, with coefficients $\{C_p^{(l)}\}$, $p = 0, 1, \ldots, 2P-1$, in the FD, (see Fig. 7.3), which partially equalizes the interference, and 2) the feedback (FB) filter, with coefficients $\{B_p^{(l)}\}$, $p = 0, 1, \ldots, 2P-1$, and output $\{Z_p^{(l)}\}$ in the FD (see Fig. 7.4), which removes part of the residual interference.
In details, $2P$-size blocks of x_i are transformed by DFT and then multiplied by the FF filter coefficients in the FD obtaining signal

$$Y_p^{(l)} = C_p^{(l)} X_p\,, \quad p = 0, 1, \ldots, 2P-1. \tag{7.10}$$

Then the output of the FB filter is summed to the FF output to obtain $U_p^{(l)} = Y_p^{(l)} + Z_p^{(l)}$. Lastly, $U_p^{(l)}$ is transformed by IDFT into $\{u_i^{(l)}\}$, which is downsampled to $\{\bar{u}_m^{(l)}\}$.
With regard to the FB part of Fig. 7.4, soft detection is performed on $\bar{u}_m^{(l-1)}$. Decoding, re-encoding and bit mapping yield $\hat{a}_m^{(l-1)}$, $m = 0, 1, \ldots, M-1$. Next, $\{\hat{a}_i^{(l-1)}\}$ is extended to size P by PN insertion as d_m. By upsampling, $\{\hat{s}_i^{(l-1)}\}$ is then obtained as in (7.8). DFT follows, whose output is multiplied by the FB filter coefficients to yield $Z_p^{(l)} = B_p^{(l)} \hat{S}_p^{(l-1)}$ for $p = 0, \ldots, 2P-1$.
Since $Z_p^{(l)}$ depends upon the detected data at iteration $(l-1)$, for $l = 1$, when no detected data is available, we set

$$\hat{a}_m^{(0)} = 0\,, \quad m = 0, 1, \ldots, M-1\,, \tag{7.11}$$

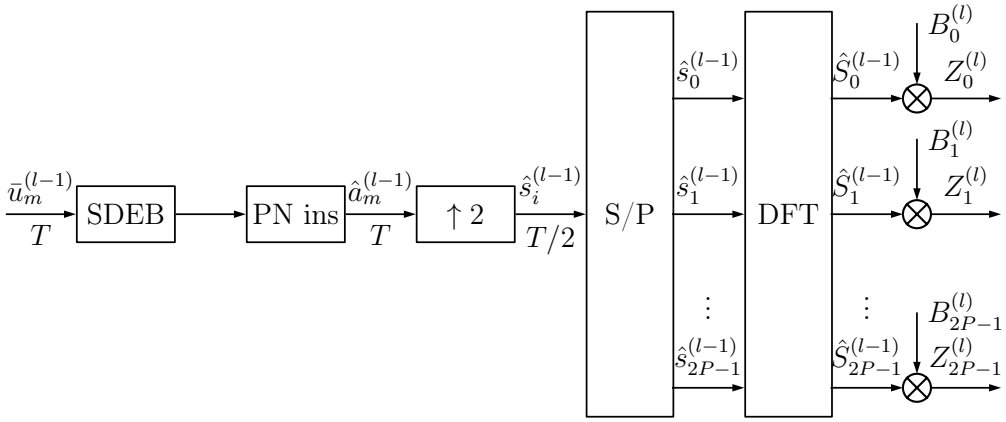

Figure 7.4: feedback part of the FS-IBDFE operating at $T/2$. SDEB: soft detection, decoding, re-encoding and bit-mapping.

while for $m = M, \ldots, P-1$, we have the PN sequence.

7.5 Design Method

As a criterion for the deign of the equalizer we consider the minimization of the MSE at the detection point, i.e.,

$$J^{(l)} = \frac{1}{P}\mathrm{E}\left[\sum_{m=0}^{P-1} |\bar{u}_m^{(l)} - a_m|^2\right] , \tag{7.12a}$$

under the constraint that the FB filter does not remove the desired component, i.e.,

$$\sum_{p=0}^{P-1} B_p^{(l)} = 0 . \tag{7.12b}$$

Since the system is independent of the FF filter gain, we add the constraint

$$\frac{1}{2P}\sum_{p=0}^{2P-1} C_p^{(l)} H_p = 1 . \tag{7.12c}$$

Now, the solution to problem (7.12) is obtained by minimizing the Lagrangian function

$$J^{(l)} + \lambda_1 \sum_{p=0}^{P-1} B_p^{(l)*} + \lambda_2 \left[\frac{1}{2P}\sum_{p=0}^{2P-1} C_p^{(l)*} H_p^* - 1\right] , \tag{7.13}$$

with respect to FF and FB coefficients, where λ_1 and λ_2 are the Lagrange multipliers such that (7.12b) and (7.12c) hold. We now provide an expression of $J^{(l)}$ as a function of the filter coefficients, and then derive a closed form solution to the minimization of (7.13).

7.5.1 MSE Computation

First, by using the Parseval's theorem we obtain

$$J^{(l)} = \frac{1}{P^2}\sum_{p=0}^{P-1} J_p^{(l)}\,, \tag{7.14}$$

where $J_p^{(l)} = \mathrm{E}[|\bar{U}_p^{(l)} - \bar{S}_p|^2]$. Note that, due to upsampling (7.8), S_p is periodic of period P, and $\bar{S}_p = S_p$, while due to downsampling

$$\bar{U}_p^{(l)} = \frac{U_p^{(l)} + U_{p+P}^{(l)}}{2}\,, \quad \bar{S}_p = \frac{S_p + S_{p+P}}{2}\,. \tag{7.15}$$

Let $M_{\hat{\mathrm{S}}}^{(l-1)}$ be the statistical power of $\hat{S}_p^{(l-1)}$, $M_{\mathrm{S}} = PM_{\mathrm{a}}$ be the power of S_p, with M_{a} the power of a_m and let

$$M_{\mathrm{W^{(IN)}}} = 2PM_{\mathrm{w^{(IN)}}} = 2PN_0 2/T, \tag{7.16}$$

with $M_{\mathrm{w^{(IN)}}}$ the power of $w_i^{(\mathrm{IN})}$. Let us define the average correlation between S_p and $\hat{S}_p^{(l-1)}$ as $r_{\mathrm{S}\hat{\mathrm{S}}}^{(l-1)} = \mathrm{E}[S_p \hat{S}_p^{(l-1)*}]$, for which estimation method [28, eq. (44)] is used, where all signals are at T. Hence, when working at $T/2$ we assume the received signal and the channel frequency response are given by, respectively, $X_p^{(T)} = (X_p^{(T/2)} + X_{P+p}^{(T/2)})/2$, $H_p^{(T)} = (H_p^{(T/2)} + H_{P+p}^{(T/2)})/2$, $p = 0, 1, \ldots, P-1$, with obvious meaning of the signals. Expanding (7.14) and using the definitions of power and correlation, $J^{(l)}$ can be rewritten as

$$\begin{aligned} J^{(l)} =& \frac{1}{P^2}\sum_{p=0}^{P-1}\Bigg\{\left|\frac{C_p^{(l)}H_p + C_{p+P}^{(l)}H_{p+P}}{2} - 1\right|^2 M_{\mathrm{S}} + \left|\frac{B_p^{(l)} + B_{p+P}^{(l)}}{2}\right|^2 M_{\hat{\mathrm{S}}}^{(l)} \\ &+ 2\Re\left[\left(\frac{C_p^{(l)}H_p + C_{p+P}^{(l)}H_{p+P}}{2} - 1\right)\left(\frac{B_p^{(l)} + B_{p+P}^{(l)}}{2}\right)^* r_{\mathrm{S}\hat{\mathrm{S}}}^{(l)}\right] \\ &+ M_{\mathrm{W^{(IN)}}}\frac{|C_p^{(l)}G_p|^2 + |C_{p+P}^{(l)}G_{p+P}|^2}{4}\Bigg\}. \end{aligned} \tag{7.17}$$

Note that the FB coefficients in (7.17) appear as $\frac{B_p+B_{p+P}}{2}$. Hence, we assume $B_p = B_{p+P}$, i.e., B_p is a periodic sequence of period P, inline with the fact that the FB filter in the time domain is working at T rather than at $T/2$. Therefore, defining matrix $\boldsymbol{R}_p^{(l)}$ and vectors $\boldsymbol{q}_p^{(l)}$, $\boldsymbol{z}_p^{(l)}$ as

$$\boldsymbol{R}_p^{(l)} = \begin{bmatrix} \frac{|H_p|^2}{4}M_S + \frac{|G_p|^2}{4}M_{\mathrm{W}} & \frac{H_p^* H_{p+P}}{4}M_{\mathrm{S}} & \frac{H_p^*}{2}r_{\mathrm{S}\hat{\mathrm{S}}}^{(l-1)*} \\ \frac{H_p H_{p+P}^*}{4}M_{\mathrm{S}} & \frac{|H_{p+P}|^2}{4}M_S + \frac{|G_{p+P}|^2}{4}M_{\mathrm{W}} & \frac{H_{p+P}^*}{2}r_{\mathrm{S}\hat{\mathrm{S}}}^{(l-1)*} \\ \frac{H_p}{2}r_{\mathrm{S}\hat{\mathrm{S}}} & \frac{H_{p+P}}{2}r_{\mathrm{S}\hat{\mathrm{S}}}^{(l-1)} & M_{\hat{\mathrm{s}}}^{(l-1)} \end{bmatrix}, \tag{7.18}$$

$$\boldsymbol{q}_p^{(l)} = \begin{bmatrix} \frac{H_p^*}{2}M_{\mathrm{S}} \\ \frac{H_{p+P}^*}{2}M_{\mathrm{S}} \\ r_{\mathrm{S}\hat{\mathrm{S}}}^{(l-1)} \end{bmatrix} \tag{7.19}$$

and

$$\boldsymbol{z}_p^{(l)} = \begin{bmatrix} C_p^{(l)} \\ C_{p+P}^{(l)} \\ B_p^{(l)} \end{bmatrix}, \tag{7.20}$$

we obtain a compact expression of $J_p^{(l)}$ as a function of the equalizer coefficients as

$$J_p^{(l)} = \boldsymbol{z}_p^{(l)H} \boldsymbol{R}_p^{(l)} \boldsymbol{z}_p^{(l)} - \boldsymbol{z}_p^{(l)H} \boldsymbol{q}_p^{(l)} - \boldsymbol{q}_p^{(l)H} \boldsymbol{z}_p^{(l)} + M_{\mathrm{S}} \,. \tag{7.21}$$

7.5.2 Minimum MSE Equalizer Coefficients

For minimizing (7.13) we set its gradient w.r.t. $\boldsymbol{z}_p$ to zero and obtain from (7.21)

$$\boldsymbol{R}_p^{(l)} \boldsymbol{z}_p^{(l)} - \boldsymbol{q}_p^{(l)} + \begin{bmatrix} \lambda_2 H_p^*/(2P) \\ \lambda_2 H_{p+P}^*/(2P) \\ \lambda_1 \end{bmatrix} = \begin{bmatrix} 0 \\ 0 \\ 0 \end{bmatrix}, \tag{7.22}$$

$p = 0, \ldots, P-1$. By solving (7.22) (7.12b) and (7.12c) w.r.t. the FB filter coefficients, we get

$$B_p^{(l)} = -\frac{r_{\mathrm{S}\hat{\mathrm{S}}}^{(l-1)}}{M_{\hat{\mathrm{S}}}^{(l-1)}} \left[\frac{C_p^{(l)} H_p + C_{p+P}^{(l)} H_{p+P}}{2} - 1 \right]. \tag{7.23}$$

Inserting now (7.23) into (7.22), and defining

$$\zeta^{(l-1)} = 1 - \frac{|r_{\mathrm{S}\hat{\mathrm{S}}}^{(l-1)}|^2}{M_{\hat{\mathrm{S}}}^{(l-1)} M_{\mathrm{S}}}, \tag{7.24}$$

$$\gamma_p^{(l)} = |H_p|^2 \zeta^{(l-1)} + |G_p|^2 \frac{M_{\mathrm{W}}}{M_{\mathrm{S}}}, \tag{7.25}$$

$$\boldsymbol{L}_p^{(l)} = \begin{bmatrix} \gamma_p^{(l)} & H_p^* H_{p+P} \zeta^{(l-1)} \\ H_p H_{p+P}^* \zeta^{(l-1)} & \gamma_{p+P}^{(l)} \end{bmatrix} \tag{7.26}$$

the optimum FF coefficients solve the system of equations

$$\alpha^{(l)} \boldsymbol{L}_p^{(l)} \begin{bmatrix} C_p^{(l)} \\ C_{p+P}^{(l)} \end{bmatrix} = \begin{bmatrix} H_p^* \\ H_{p+P}^* \end{bmatrix} \tag{7.27}$$

where $\alpha^{(l)}$ is such that (7.12c) is satisfied. Hence, for $p = 0, \ldots, 2P-1$, we write

$$C_p^{(l)} = \frac{\kappa_p^{(l)}}{\alpha^{(l)}}, \qquad \alpha^{(l)} = \frac{1}{2P} \sum_{p=0}^{2P-1} H_p \kappa_p^{(l)}, \tag{7.28}$$

and various expressions of $\kappa_p^{(l)}$ are obtained according to the properties of $\boldsymbol{L}_p^{(l)}$. Here we focus on the case in which H_p and G_p have the same support and we consider the two cases in which $\det(\boldsymbol{L}_p) \neq 0$ and $\det(\boldsymbol{L}_p) = 0$.

Case $\det(\boldsymbol{L}_p) \neq 0$ **for** $H_p \neq 0$ **and** $H_{p+P} \neq 0$ In this case we have

$$\kappa_p^{(l)} = H_p^* |G_{p+P}|^2 \times \left[\zeta^{(l-1)} (|H_p|^2 |G_{p+P}|^2 + |H_{p+P}|^2 |G_p|^2) + \frac{M_{\mathrm{W}}}{M_{\mathrm{S}}} |G_p|^2 |G_{p+P}|^2 \right]^{-1}, \quad (7.29)$$

where $p = 0, 1, \ldots, 2P-1$ and we note that both H_p and G_p are periodic with period $2P$, i.e., $H_{p+P} = H_{p-P}$ for $p = P, \ldots, 2P-1$, and similarly for G_p.

Case $\det(\boldsymbol{L}_p) = 0$ **for** $H_p = 0$ **and any** H_{p+P} In this case, from (7.10) the best solution is

$$\kappa_p^{(l)} = 0\,, \quad \text{if } H_p = 0\,. \quad (7.30)$$

Case $\det(\boldsymbol{L}_p) = 0$ **for** $H_{p+P} = 0$ **and** $H_p \neq 0$ In this case, from (7.27) we have

$$\kappa_p^{(l)} = H_p^* (\gamma_p^{(\ell)})^{-1}\,. \quad (7.31)$$

To summarize, based upon a previous detection data block, the correlation $r_{\mathrm{S}\hat{\mathrm{S}}}^{(l-1)}$ can be estimated. Then, using $\{H_p\}$ and $\{G_p\}$, $p = 0, \ldots, 2P-1$, the FF coefficients can be determined by (7.29), (7.30), (7.31), and (7.28) with corresponding global MSE $J^{(l)}$. It is important to note that the FF coefficients, for which (7.12c) holds, the FB coefficients, as given by (7.23), automatically satisfy constraint (7.12b). Now, processing of $\{X_p\}$ and $\{\hat{S}_p^{(l-1)}\}$ can start, to yield a new signal at detection point which can be (soft) detected, decoded and re-encoded to provide $\{\hat{S}_p^{(l)}\}$ and the whole design procedure can be iterated once more. Note that the solution of the system of equations (7.22) is more involved than the solution to IBDFE [28], as can be seen from (7.29)-(7.31).

7.6 Numerical Results

For a quadrature phase shift keying (QPSK) transmission over a channel with a Rayleigh fading typical urban model [29] a square root raised cosine filter with roll-off factor 0.2 is considered at the transmitter, while an anti-aliasing filter is used at the receiver [27, 30]. We set $L = 72$ and $M = 952$. Information bits are encoded by a low density parity check (LDPC), with rate 2/3 and frame size of 64,800 bit. Over a frame, the channel is assumed known and time-invariant. The FB *output* is recursively updated as better data are produced by the cascade of the soft detector, decoder, encoder, bit mapper as in [28]. While FS-IBDFE and IBDFE of [28] update filters at each iteration, in NP-FS-FDE of [27], the FF is given by a FS-LE and the FB is working at T [30]. Note that at the first iteration FS-IBDFE and NP-FS-FDE yield the same FS-LE receiver.

Figures 7.5 and 7.6 show the cumulative distribution function (CDF) of the bit error rate (BER) for a SNR $\Gamma = 4.5$ dB, where Γ is as in (7.6). In the first it is highlighted the effect of iterations on the decoding procedure, while in the latter comparison with the other considered schemes is shown. We observe that the proposed FS-IBDFE significantly outperforms all other solutions, showing at the same time the merits of filter adaptation and FS operation at the receiver front-end. In fact, the IBDFE working at T introduces folding of the equivalent channel frequency response before the FF,

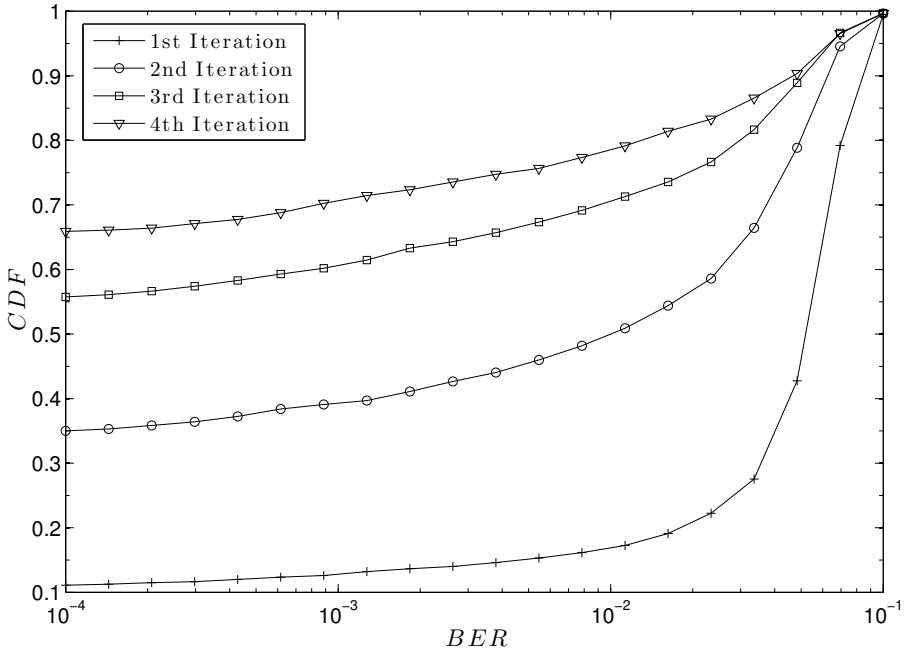

Figure 7.5: CDF of the BER for the FS-IBDFE scheme with an average SNR of 4.5 dB, at various iterations.

Structure	CMUL
IBDFE	$2C_{\text{FFT}}(P) + P + (N_I - 1)\left[2C_{\text{FFT}}(P) + 2P\right]$
FS-IBDFE	$C_{\text{FFT}}(2P) + 2P + C_{\text{FFT}}(P) + (N_I - 1)\left[2C_{\text{FFT}}(P) + 3P\right]$
NP-FS-FDE	$C_{\text{FFT}}(2P) + 2P + C_{\text{FFT}}(P) + (N_I - 1)\left[2C_{\text{FFT}}(P) + P\right]$

Table 7.1: Computational complexity of the system in terms of number of complex multiplications (CMUL) per data block. N_I is the number of iterations and $C_{\text{FFT}} = P/2 \log_2 P - P$ is the number of CMULs for an FFT of size P [28].

and this increases ISI. Moreover, filters of the NP-FS-FDE are designed assuming that the data is known and are fixed for a given channel. Hence, the whole structure does not make use on available information on data. Complexity of FS-IBDFE is higher than that of the other two structures, as reported in Table 7.1. For example, with $P = 1,024$, at iteration one the FS structures have complexity 1.6 w.r.t. the IBDFE operating at T. When more iterations are considered, the complexity of all structures is very similar, e.g., the complexity of FS-IBDFE and NP-FS-FDE are 1.2 and 1.1 times w.r.t. to IBDFE at $N_I = 4$ iterations, as can be seen from Table 7.2. On the other hand, for the design complexity, the NP-FS-FDE must solve a linear system of equations [30], while both FS-IBDFE and IBDFE require simple multiplications and divisions.

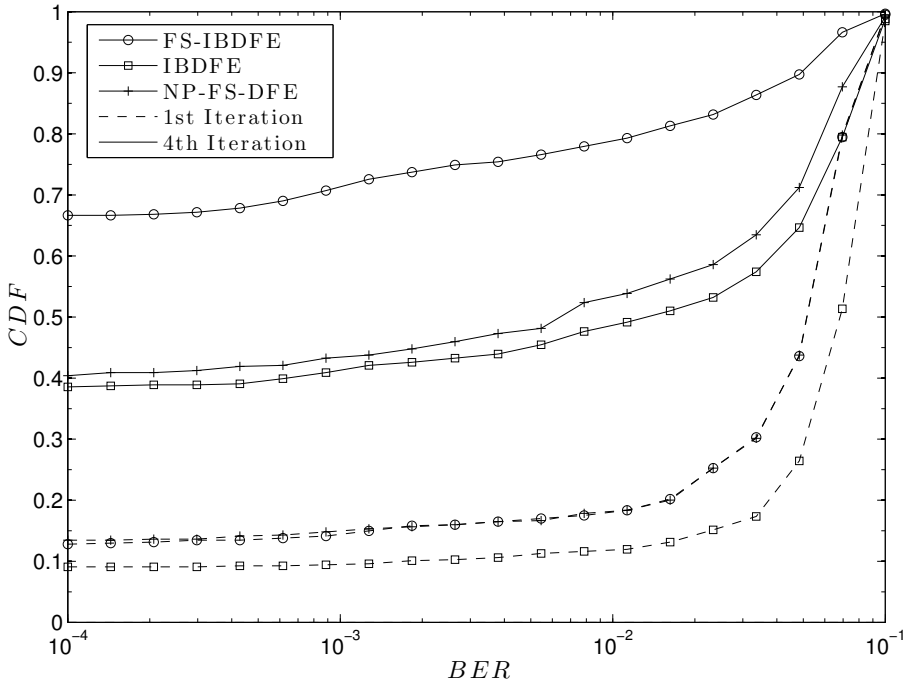

Figure 7.6: CDF of the BER for various equalization schemes with an average SNR of 4.5 dB, at iteration one (dashed lines) and iteration four (solid lines).

	IBDFE	FS-IBDFE	NP-FS-FDE
$N_I = 1$	9216	15360	15360
$N_I = 2$	19456	26624	24576
$N_I = 3$	29696	37888	33792
$N_I = 4$	39936	49152	43008

Table 7.2: Number of complex multiplications involved in the considered structures, at different iterations. $P = 1024$.

Chapter 8

Conclusions

We analysed the problem of multiplexing several users over the same physical channel using the interference alignment technique. This method ortogonalizes the signal subspace spanned by the interfering signals coming from other users with the one in which the intended signal is transmitted. Particular attention has been given to the performance achieved by these algortithms over the MMW channel.

The results obtained with the MMW channel are encouraging for the future development of next generation mobile networks over this band. The algorithms already proposed for the classic Rayleigh fading channel behave quite well also in the MMW scenario and provide therefore a start point for future improvements. In particular, the peculiarity of the modes highlighted in Chapter 6 suggests that resource allocation can be a relevant operation to optimize the filter design. In fact, waterfilling is a powerful algorithm for power allocation in MIMO systems, but its effectiveness is limited to situations where interference is completely removed, which is not always the case. Moreover, cooperation between BSs can better exploit the limited degrees of freedom offered by the MMW channel, since as we saw the considered algorithms suffer in the downlink scenario where cross-channels are equal to the direct channel. A further performance evaluation could be the simulation of a urban environment that takes into account different distances between user and BSs as well as different fading statistics due to obstacles or other particular conditions.
Furthermore, the new properties of the channel could be taken into account in the design procedure of the RF part and of higher protocol stack levels, like medium access schemes, since the narrow beam generated by the antenna arrays can make possible a space-based division of the channel and many assumptions made in modern wireless systems may be a limitation of the actual possibilities given by this new spectrum.

Finally, during my thesis I was also involved on a different research topic: how to design a frequency domain equalizer for wideband channels, focusing in particular on the FS-IBDFE, that allows a closed form expression of the equalizer coefficients. Application of the FS-IBDFE solution to a typical broadband wireless transmission, shows its effectiveness over both IBDFE and NP-FS-FDE, at the cost of a slightly higher complexity.

Appendix A

Waterfilling Algorithm

The waterfilling algorithm is a widely used method for power allocation in systems where data symbols are transmitted via multiple sub-channels that experience different fading. The name of the algorithm suggests the idea behind it, that is to compensate channel impairments by assign to each subchannel the amount of power needed to reach a reference level common to all channles, in the same way water finds its level when filled in one of several communicating vessels.

Assume then to have a channel which consist of a set of N_c non-interfering sub-channels, each corrupted by independent noise, called *parallel channel*, and a sum power constraint that has to be met. We want allocate power to each sub-channel, as stated in (3.2), such that the total power constraint P is met. For a given set of power allocated P_n, $n = 0, ..., N_c - 1$, the maximum rate of reliable communication is

$$\sum_{n=0}^{N_c-1} \log\left(1 + \frac{P_n|\tilde{h}_n|^2}{N_0}\right) \qquad bits/channel\ use, \tag{A.1}$$

being $\tilde{h}_n$ the n-th sub-channel gain and N_0 the noise PSD.
In order to maximize Eq. (A.1), we can find the optimal power allocation by solving the optimization problem

$$C_{N_c} = \max_{P_0,..,P_{N_c-1}} \sum_{n=0}^{N_c-1} \log\left(1 + \frac{P_n|\tilde{h}_n|^2}{N_0}\right), \tag{A.2}$$

subject to

$$\sum_{n=0}^{N_c-1} P_n = P, \qquad P_n \geq 0, \qquad n = 0, ..., N_c - 1. \tag{A.3}$$

The optimal power allocation can be explicitly found by Lagrangian methods since the objective function in (A.2) is jointly concave in the powers. Consider then the Lagrangian

$$\mathcal{L}(\bar{\lambda}, P_0, ..., P_{N_c-1}) = \sum_{n=0}^{N_c-1} \log\left(1 + \frac{P_n|\tilde{h}_n|^2}{N_0}\right) - \bar{\lambda} \sum_{n=0}^{N_c-1} P_n, \tag{A.4}$$

being $\bar{\lambda}$ the Lagrangian multiplier. The Kuhn-Tucker condition for the optimality of a power allocation is

$$\frac{\delta \mathcal{L}}{\delta P_n} \begin{cases} = 0 & if P_n > 0 \\ \leq & if P_n = 0. \end{cases} \tag{A.5}$$

By defining $x^+ = max(x, 0)$, the optimal power level for subchannel n are given by the following

$$P_n^* = \left(\frac{1}{\bar{\lambda}} - \frac{N_0}{|\tilde{h}_n|^2} \right)^+, \tag{A.6}$$

where the Lagrangian multiplier $\bar{\lambda}$ has to be chosen such that the power constraint is met:

$$\sum_{n=0}^{N_c-1} \left(\frac{1}{\bar{\lambda}} - \frac{N_0}{|\tilde{h}_n|^2} \right)^+ = P. \tag{A.7}$$

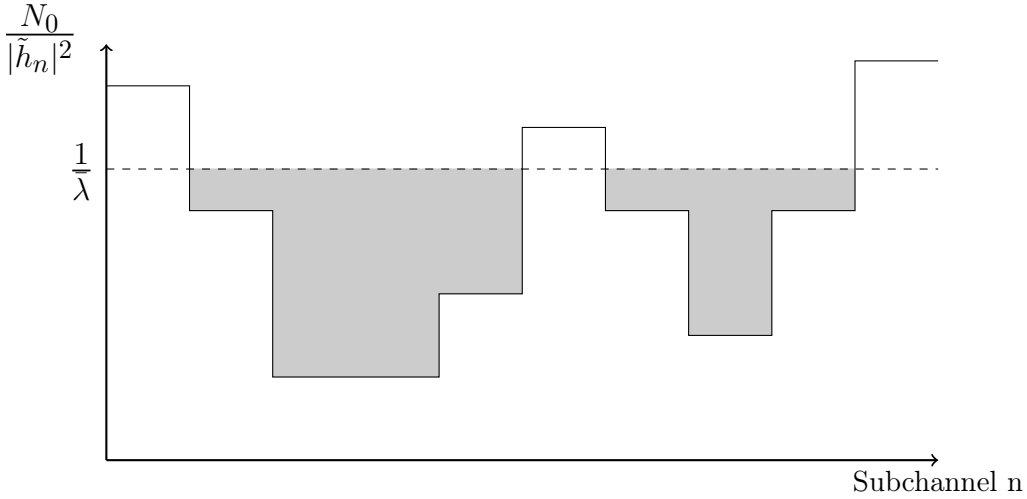

Figure A.1: Waterfilling power allocation for N_c sub-channels

We can now explain this methody using the analogy of water pouring. In Figure A.1 a pictorial view of the optimal power allocation strategy is given. Think of the sub-channels as many vessels where the value $N_0/|\tilde{h}_n|^2$, plotted as a function of the subchannel index in Fig. A.1, represent the bottom level. If we pour P units of water into our vessels, that are communicating, the height of the water surface in every vessel is equal to $1/\bar{\lambda}$. From this analogy cames the name waterfilling. Note that there might be some sub-channels where the bottom of the vessel is above the water and no power is allocated to them. In these sub-channels, the gain is too poor to be worthwhile to transmit information. In general, the transmitter allocates more power to the stronger sub-channels, taking advantage of the better gain level, and less or even no power to the weaker ones. To find more informations, refer to [8].

In MIMO systems, waterfilling allocates power among the modes of the equalized channel matrix, that is, the equivalent channel matrix after beamforming and combining is applied. If both intra-user and inter-user interference is removed, we have

$$(\mathbf{U})^H \mathbf{HV} = diag\{\lambda_1, ..., \lambda_d\}, \tag{A.8}$$

being λ_i the eigenvalues of $\mathbf{HH}^H$ and thus the gains relative to the different modes. We can therefore set $\lambda_i = |\tilde{h}_i|^2$ and apply the algorithm to the virtual subchannels provided by the different modes of the MIMO channel matrix. In Algorithm 4 it is presented the pseudo-code for the optimal power allocation choise provided by waterfilling.

Algorithm 4 Waterfilling

Initialization:

Let r be the number of modes (virtual subchannel), sorted in descending order w.r.t. the SNR level.

$$\mu \leftarrow \frac{1}{r}\left[P + \sum_{i=1}^{r} \frac{N_0}{\lambda_i}\right] \tag{A.9}$$

$$P_i \leftarrow \mu - \frac{N_0}{\lambda_i}, \qquad i = 1, ..., r \tag{A.10}$$

$m \leftarrow r$

Procedure:

while $P_i > 0$, $i = 1, ..., m$ **do**

$$\mu \leftarrow \frac{1}{m}\left[P + \sum_{i=1}^{m} \frac{N_0}{\lambda_i}\right] \tag{A.11}$$

$$P_i \leftarrow \mu - \frac{N_0}{\lambda_i}, \qquad i = 1, ..., m \tag{A.12}$$

$$P_i \leftarrow 0, \qquad i = m+1, ..., r \tag{A.13}$$

    if $\exists\ P_i \leq 0$, $i = 1, ..., m$ **then**
        $m \leftarrow m - 1$
    end
end
    return P_i, $i = 1, ..., r$

Appendix B

Non-FS Iterative Block DFE

The IBDFE scheme is equivalent counterpart of the FS-IBDFE with sampling rate equal to the symbol period, i.e. $T_s = T$, as can be seen in Figures B.1 and B.2. In this case, the MSE at detection point is given by

$$J^{(l)} = \frac{1}{P}\mathrm{E}\left[\sum_{m=0}^{P-1} |\bar{u}_m^{(l)} - a_m|^2\right] \tag{B.1}$$

that, after applying Parseval's theorem and taking the expectation, becomes

$$\begin{aligned} J^{(l)} =& \frac{1}{P^2}\sum_{p=0}^{P-1} \left|C_p^{(l)}\right| M_{\mathrm{W}^{(\mathrm{IN})}} \\ &+ |C_p^{(l)}H_p - 1|^2 M_{\mathrm{S}} + |B_p^{(l)}|^2 M_{\hat{\mathrm{S}}}^{(l-1)} \\ &+ 2\Re\left[B_p^{(l)*}\left(C_p^{(l)}H_p - 1\right) r_{\mathrm{S}\hat{\mathrm{S}}}^{(l-1)}\right]. \end{aligned} \tag{B.2}$$

The minimization of (B.2) yields the solution for the FF filter, given by

$$C_p^{(l)} = \frac{k_p^{(l)}}{\frac{1}{P}\sum_{k=0}^{P-1} H_k \kappa_k^{(l)}}, \qquad p = 0, 1, \cdots, P-1 \tag{B.3}$$

where

$$k_p^{(l)} = \frac{H_p^*}{M_W|G_p|^2 + M_S\left(1 - \frac{\left|r_{S\hat{S}}\right|^2}{M_{\hat{S}} M_S}\right)|H_p|^2}. \tag{B.4}$$

The FB filter will have instead coefficients equal to

$$B_p^{(l)} = -\frac{r_{S\hat{S}}^{(l-1)}}{M_{\hat{S}}}\left[H_p C_p^{(l)} - 1\right], \qquad p = 0, 1, \cdots, P-1. \tag{B.5}$$

We remark that at $T_s = T$, the noise power in the FD is given by

$$M_{\mathrm{W}^{(\mathrm{IN})}} = P M_{\mathrm{w}^{(\mathrm{IN})}} = P N_0 / T. \tag{B.6}$$

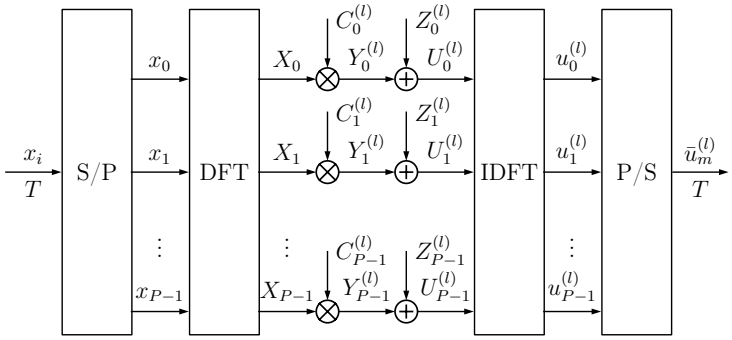

Figure B.1: feedforward part of the IBDFE operating at T.

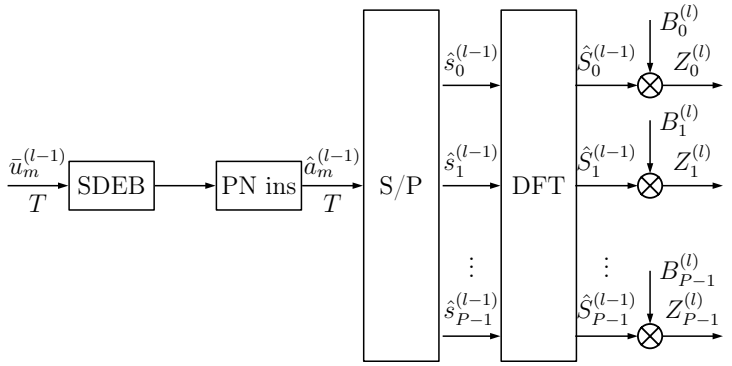

Figure B.2: feedback part of the IBDFE operating at T. SDEB: soft detection, decoding, re-encoding and bit-mapping.

Appendix C

Noise Prediction DFE

A different feedback configuration from the one presented in Chapter 7 involves the employment of a noise prediction filter. If we assume $\hat{a}_m^{(l)} = a_m$, the input of the feedback filter, that is $d_m = \hat{a}_m^{(l)} - a_m$, is colored noise. By removing the correlated noise e_m from s_m, we obtain y_m that is composed of white noise, with minimum variance, plus desired symbol a_m [31]. The system configuration is shown in Fig. C.1, where the linear equalizer in the FD is determined as follow.
Let

$$\bar{C}_p = \frac{H_p^*}{(|H_p|^2 + |H_{p+P}|^2) + \frac{M_W}{M_S}}. \qquad p = 0, \cdots, 2P-1, \tag{C.1}$$

and

$$\alpha = \frac{1}{2P} \sum_{k=0}^{2P-1} H_k \bar{C}_k, \tag{C.2}$$

it is

$$C_p = \frac{\bar{C}_p}{\alpha} \qquad p = 0, \cdots, 2P-1. \tag{C.3}$$

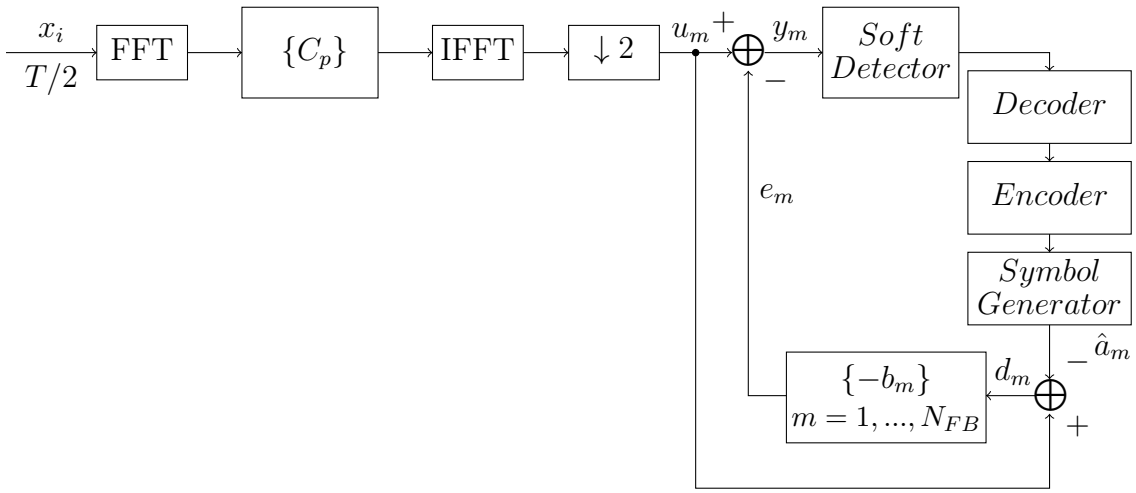

Figure C.1: NP-DFE system configuration

The noise prediction as a feedback filter of length $N_{FB} = L - 1$, with coefficients $[0, -b_1, \cdots, -b_{FB}]$, can be found instead by the following system of equations

$$\sum_{m=1}^{N_{FB}}(-b_m)q_{n-m} = q_n, \quad n = 1, \cdots, N_{FB} \tag{C.4}$$

where $\mathbf{q} = \{q_0, \cdots, q_{P-1}\}$ is the $IDFT$ of

$$Q_p = \frac{1}{|H_p|^2 + |H_{p+P}|^2 + \frac{M_W}{M_S}} \qquad p = 0, \cdots, P-1 \tag{C.5}$$

If we denote with bold letters the vector given by the symbols of the whole transmission block, i.e. $\mathbf{x} = \{x_1, x_2, ..., x_{P-1}\}$, the data sequence, after the $IDFT$, is downsampled to yeld the vector $\mathbf{s}$ of length P.
The noise predictor will then predict interference due to preceding symbols from the coloured noise affecting received signal. That is,

$$\mathbf{e} = \mathbf{B} \cdot \mathbf{d} \tag{C.6}$$

where $\mathbf{B}$ is a $P \times P$ circular matrix whose first row is equal to

$$\mathbf{B}_{[1,:]} = [0 \ \cdots \ 0 \ -b_{N_{FB}} \ -b_{N_{FB}-1} \ \cdots \ -b_1]\,. \tag{C.7}$$

The sequence that is being passed to the detector is then given by

$$\mathbf{y} = \mathbf{u} - \mathbf{e} = \mathbf{u} - \mathbf{B} \cdot \mathbf{d} = \mathbf{u} - \mathbf{B}\,(\mathbf{u} - \hat{\boldsymbol{a}}) \tag{C.8}$$

from which the new estimated sequence is obtained and a new iteration can be performed.

Bibliography

[1] Ericsson Mobility Report 2004.

[2] S. Rangan, T.S. Rappaport and E. Erkip, "Millimeter-Wave Cellular Wireless Networks: Potentials and Challenges," *Proceedings of the IEEE*, 2014.

[3] C. Anderson, T.Rappaport, "In-Building Wideband Partition Loss Measurements at 2.5 and 60 GHz," *IEEE Transactions on Wireless Communications*, 2004.

[4] A. Alejos, M. Sanchez and I. Cuinas, "Measurement and Analysis of Propagation Mechanisms at 40 GHz: Viability of Site Shielding Forced by Obstacles," *IEEE Transactions on Vehicular Technology*, 2008.

[5] P. Smulders, L. Correia, "Characterisation of propagation in 60 GHz radio channels," *Electronics and Communication Engineering Journal*, 1997.

[6] Z. Pi, F. Khan, "An introduction to millimeter-wave mobile broadband systems," *IEEE Communications Magazine*, 2011.

[7] P. Baracca, F. Boccardi and N. Benvenuto, "A dynamic clustering algorithm for downlink CoMP systems with multiple antenna UEs," *Journal on Wireless Communications and Networking*, 2014.

[8] D.Tse, P.Viswanath, *Fundamentals of Wireless Communication.* Cambridge University Press, 2005.

[9] H. Xu, T.S. Rappaport, R.J. Boyle and J.H. Schaffner, "Measurements and Models for 38-GHz Point-to-Multipoint Radiowave Propagation," *IEEE Journal on Selected Areas in Communications*, 2000.

[10] O. Ayach, R. Heath, S. Abu-Surra, S. Rajagopal and Z. Pi, "Low complexity precoding for large millimeter wave MIMO systems," *IEEE Communications Magazine*, 2011.

[11] F. Khan, Z. Pi, "mmWave mobile broadband (MMB): Unleashing the 3-300GHz spectrum," *34th IEEE Sarnoff Symposium*, 2011.

[12] V. Cadambe, S. Jafar, "Interference Alignment and Degrees of Freedom of the K-User Interference Channel," *IEEE Trans. on Information Theory*, 2008.

[13] K. Gomadam, V. R. Cadambe and S. A. Jafar, "Approaching the Capacity of Wireless Networks through Distributed Interference Alignment," *IEEE GLOBECOM*, 2008.

[14] H. Ghauch, C. Papadias, "Interference Alignment: a one sided approach," *IEEE GLOBECOM*, 2011.

[15] D. A. Schmidt, C. Shi, R. A. Berry, M. L. Honig. and W. Utschick, "Comparison of Distributed Beamforming Algorithms for MIMO Interference Networks," *IEEE Trans. on Signal Processing*, 2013.

[16] J. H. Winters, "Optimum Combining in Digital Mobile Radio with Cochannel Interference," *IEEE Journal on Selected Areas in Communications*, 1984.

[17] A. G. Helmy, A. Gomaa, A. R. Hedayat and N. Al-Dahir, "Multi-Stream Sum-Rate-Maximizing Interference Alignment under Sparsity Constraints," *IEEE GLOBECOM*, 2013.

[18] A. G. Helmy, A. R. Hedayat, N. Al-Dahir, "Robust Weighted-Sum-Rate based Multi-Stream Transmission for the MIMO Interference Channel," *IEEE*, 2015.

[19] Q.H. Spencer, A.L. Swindlehurst, and M. Haardt, "Zero-Forcing Methods for Downlink Spatial Multiplexing in Multiuser MIMO Channels," *IEEE Trans. on Signal Processing*, 2004.

[20] Federico Boccardi and Howard Huang, "A near-optimum technique using linear precoding for the MIMO broadcast channel," *IEEE ICASSP*, 2007.

[21] S. W. Peters and R. W. Heath, "Cooperative Algorithms for MIMO Interference Channels," *IEEE Trans. on Vehicular Technology*, 2011.

[22] G. Ungerboek, "Adaptive maximum likelihood receiver for carrier modu- lated data transmission systems," *IEEE Trans. Commun.*, 1974.

[23] F. Pancaldi, G. Vitetta, R. Kalbasi, N. Al-Dhahir, M. Uysal, and H. Mheidat, "Single-carrier frequency domain equalization," *IEEE Signal Processing*, 2008.

[24] N. Benvenuto, R. Dinis, D. Falconer, and S. Tomasin, "Single carrier modulation with nonlinear frequency domain equalization: An idea whose time has come again," *Proceedings of the IEEE*, 2010.

[25] P. Vaidyanathan and B. Vrcelj, "Theory of fractionally spaced cyclic-prefix equalizers," *IEEE ICASSP*, 2002.

[26] A. Modenini, G. Colavolpe, and N. Alagha, "How to significantly improve the spectral efficiency of linear modulations through time-frequency packing and advanced processing," *Proc. IEEE Int. Conf. on Communications (ICC)*, 2012.

[27] A. Koppler, A. Springer, and R. Weigel, "Combined frequency domain feedforward and turbo decision feedback equalization for single carrier W-LAN systems," *Proc. IEEE Int. Conf. on Communications (ICC)*, 2003.

[28] S. Tomasin and N. Benvenuto, "Iterative design and detection of a DFE in the frequency domain," *IEEE Trans. Commun.*, 2005.

[29] ETSI report. Universal Mobile Telecommunications System (UMTS); Deployment aspects (3GPP TR 25.943 version 12.0.0 Release 12). ETSI TR 125 943 V12.0.0

[30] Y. Zhu and K. B. Letaief, "Single carrier frequency domain equalization with noise prediction for broadband wireless systems," *Proc. IEEE Globecom*, 2004.

[31] N. Benvenuto and G. Cherubini, *Algorithms for Communications Systems and Their Applications*. Wiley, 2002.